COGNITIVE FUNCTION EVALUATION FOLLOWING A CERVICAL SPINAL CORD INJURY: A CASE STUDY THROUGH THE MIDDLE CEREBRAL ARTERIES USING TRANSCRANIAL DOPPLER

by

Héloïse Bleton

B.S. in Electrical Engineering, INSA Lyon, 2014

Submitted to the Graduate Faculty of

the Swanson School of Engineering in partial fulfillment

of the requirements for the degree of

Master of Science

University of Pittsburgh

2014

UNIVERSITY OF PITTSBURGH

SWANSON SCHOOL OF ENGINEERING

This thesis was presented

by

Héloïse Bleton

It was defended on

July 8th 2014

and approved by

Ervin Sejdić, Ph. D., Assistant Professor

Department of Electrical and Computer Engineering

Luis F. Chaparro, Ph. D., Associate Professor

Department of Electrical and Computer Engineering

Zhi-Hong Mao, Ph. D., Associate Professor

Department of Electrical and Computer Engineering

Thesis Advisor: Ervin Sejdić, Ph. D., Assistant Professor

Department of Electrical and Computer Engineering

COGNITIVE FUNCTION EVALUATION FOLLOWING A CERVICAL SPINAL CORD INJURY: A CASE STUDY THROUGH THE MIDDLE CEREBRAL ARTERIES USING TRANSCRANIAL DOPPLER

Héloïse Bleton, M.S.

University of Pittsburgh, 2014

Spinal cord injury (SCI) is one of the most common neurological disorders. In this paper, we examined the consequences of upper SCI in a male participant on cerebral blood flow velocity (CBFV). In particular, transcranial Doppler (TCD) was used to study these effects through middle cerebral arteries (MCA) during resting-state periods and during cognitive challenges (non-verbal word-generation tasks and geometric-rotation tasks). Signal characteristics were analyzed from raw signals and envelope signals (maximum velocity) in time domain, frequency domain and time-frequency domain. Frequency features pointed out an increase of peak frequency in L-MCA and R-MCA raw signals which revealed stronger cerebral blood flow during geometric/verbal processes respectively. This underlined a slight dominance of the right hemisphere during word-generation periods and a slight dominance of the left hemisphere during geometric processes. This finding was confirmed by cross-correlation in time domain and by entropy rate in information-theoretic domain. Comparing our results to other neurological disorders (Alzheimer's disease, Parkinson's disease, autism, epilepsy, traumatic brain injury) showed that the SCI had similar effects such as a general decreased cerebral blood flow and similar regular hemispheric dominance in a few cases.

Keywords: transcranial Doppler, spinal cord injury, cognitive tasks, cerebral blood flow velocity.

TABLE OF CONTENTS

LIST OF TABLES

LIST OF FIGURES

PREFACE

I would like to thank Dr. Mahmoud El Nokali for giving me the chance to study in the Swanson School of Engineering. I would like to express my greatest gratitude to my advisor Dr. Ervin Sejdić who has given a welcoming attitude and useful guidance. I am also very grateful to my colleagues and my family for their support and their help during my master studies. I am also very grateful to the participant for the amount of time spent collecting data.

1.0 INTRODUCTION

1.1 FUNCTIONAL BRAIN IMAGING

1.1.1 Brain imaging methods

Brain response to mental or physical performance is a key area in cognitive neuroscience research. Nowadays, functional brain imaging techniques include positron emission tomography (PET), functional magnetic resonance imaging (fMRI), computed tomography (CT), single photon emission computed tomography (SPECT), electroencephalography (EEG), magnetoencephalography (MEG) and near infrared spectroscopy (NIRS) [1]. All these procedures are used to map functional regional changes in brain activity, i.e. regional brain circulation, metabolism and electrical activity [2]. Most of them collect functional brain imaging signals and establish correlation between regional changes in cerebral perfusion and neural activation (PET, fMRI, SPECT) [3], [4]. At first sight, cerebral blood flow changes may serve to adjust glucose and oxygen rates in response to brain energy demands. This idea now appears oversimple [5]. In fact, cerebral blood flow is controlled locally by glutamate. This amino-acid is a part of neuronal activation for producing some agents (nitric oxide, adenosine and arachidonic acid metabolites) [6]. These agents contribute to a blood vasodilatation which stretches to surrounding areas through a local parallel fiber network [7]. It gives explanation about blood flow increases over large regions (not only at the level of brain activated regions) [6]. Physiologist Angelo Mosso first described a functional change in local blood flow circulation during a mental arithmetic challenge [5], [8]. He noticed that brain pulsations increased while continuously measuring brain activity over the right prefrontal cortex through the defective skull of one subject. In the following century, neuroimaging

research focused on local changes of cerebral blood flow at the sites of brain activation. Additionally, multiple studies confirmed Mosso's statement about changes in local distribution of patterns of blood perfusion through main cerebral arteries. However, in the past few years, PET and fMRI were typically used to investigate hemodynamic changes. Examining human brain behaviors in health or disease with PET then with fMRI contributes to the expansion of a new scientific sector called cognitive neuroscience [5]. Figure 1 summarizes PET and fMRI general chronology.

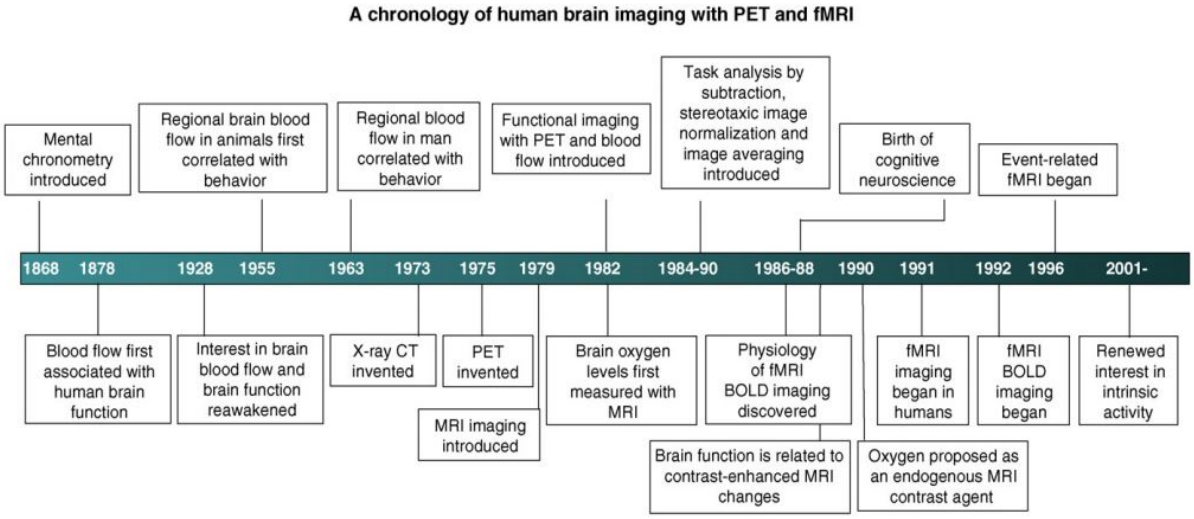

Figure 1: A chronology of major events associated with functional brain mapping concerning PET and fMRI; adapted from Raichle [9]

1.1.2 Transcranial Doppler

Local distribution of patterns of blood perfusion can be described by other neuroimaging methods. The hemodynamic features of main cerebral arteries and their rapid variations can be characterized by transcranial Doppler. Aaslid, Markwalder and Nornes introduced the transcranial Doppler sonography into clinical practice as a non-invasive ultrasonic technique to measure cerebral blood flow velocity and its variations [10]. TCD measured activities in main cerebral arteries through an intact skull in normal and pathological conditions [10], [11]. This technique uses the fact that cerebral perfusion is linked to neural activation which

is translated into cerebral perfusion changes during cognitive tasks [3], [4]. The velocity measurement is closely linked to cerebral blood flow in the event that the diameter of cerebral arteries does not change during the insonation. Multiple studies showed that perfusion area and diameter of cerebral arteries do not change during mental processes [12], [13], [14]. Thus, blood flow velocity evolutions are due to modifications in cerebral metabolism because of cerebral activities.

TCD has been studied during mental/cognitive or physical tasks for both healthy participants and patients affected by neurological disorders (e.g., stroke, autism, epilepsy) [15], [16], [17], [18], [19]. Previous publications have examined the effects of visual perception [20], [21], auditory perception [22], [23], language processes [24], [25], spatial processes [26], [27], memory processes [28], other cognitive/mental tasks and other neurological disorders [17], [29], [30] on cerebral blood flow using TCD.

1.1.3 Comparison of functional brain imaging techniques

This research is focused on non-invasive or partially invasive functional brain imaging techniques which examine cerebral blood flow evolution. Comparing advantages and disadvantages of brain imaging mapping is a main point for demonstrating the importance of TCD feasibility. We consider non-invasive or partially invasive neuroimaging methods such as PET, fMRI and SPECT. We also add characteristics of TCD. We exclude techniques which measure the electrical activity of the brain. Table 1 exhibits respective advantages and disadvantages of each method.

Generally, these methods have a high spatial resolution. Despite their advantages, these methods expose patients in an uncomfortable way: their movements, which cannot change between two sets of images, are restricted. The second disadvantage of these techniques is their low temporal resolution. These restrictions prevent a lot of applications [32], [33], [34], [35]. On the opposite side, TCD has a high temporal resolution due to continuous insonation [36]. Previous publications pointed out that the main advantages of a TCD system include its price, easiness-to-use and its minimally stressful character [37], [38].

Table 1: Non-invasive and partially invasive brain imaging techniques; adapted from Min [31] and from Khalil [32]

Technique	Advantages	Disadvantages
PET	High sensitivity Spatial resolution Multiple natural radiotracers	Partially invasive One process evaluated at a time Difficulty with separating reaction steps Short time for scanning (short half-life time of radiotracers) Limited mobility Expensive
fMRI	Non-invasive Spatial resolution Analysis of the entire brain	Temporal resolution because of inherent hemodynamic delay Incompatible with ferro-magnetic materials Limited mobility Set-up and maintenance costs Expensive
SPECT	High sensitivity Long half-life time of radiotracers Injection of two radiotracers	Partially invasive Low temporal and spatial resolutions Inability to quantify processes with lack of attenuation correction Few radiotracers available for evaluation of metabolism Limited mobility Expensive
TCD	Non-invasive Temporal resolution Good mobility Low cost	Spatial resolution Specific areas for insonation and difficulties for finding path of insonation Targeting only arteries

1.2 SPINAL CORD INJURY

A spinal cord injury (SCI) in patients usually implies partial or full motor/sensory dysfunction [39] [40], and the severity of SCI is evaluated according to the American Spinal Injury Association Impairment Scale. Following a spinal cord lesion, physicians usually perform imaging tests to determine the vertebral level of injury. Nowadays, the magnetic resonance imaging (MRI) surpasses other imaging techniques such as X-Rays or Computer-Assisted Tomography Scans [41].

Multiple articles investigated the consequences of SCI on brain activity. The majority of these studies examined the effects of SCI on brain response during motor activity. All of them emphasized brain reorganization following a lesion in the central nervous system (CNS). Functional magnetic resonance imaging (fMRI), positron emission topography (PET), transcranial magnetic stimulation (TMS), magneticencephalography (MEG) and electroencephalography (EEG) were usually used to measure change in cerebral blood flow/ metabolic activity/ electrical activity from the brain in the case of SCI [42]. A few studies examined a link between SCI and CBFV in patients with a high level of SCI, i.e. above the sixth thoracic segment [43], [44], [45]. In particular, CBFV appeared to be lower in the case of SCI subjects when compared to control participants during resting-state periods [46]. A few of them highlighted SCI consequences on brain response during mental challenges. SCI may imply impaired response of cerebral blood flow during cognitive tasks [47], [48], [49]. Furthermore, CBFV may not increase during stimulus mental periods [46].

1.3 RESEARCH OBJECTIVE

The current study focused on examining the repercussion of the injury in the upper side of the spinal cord on CBFV. Specifically, we examined CBFV in middle cerebral arteries (MCA) during rest periods and cognitive tasks from a male SCI participant on the fifth cervical vertebra. Findings from resting-state serve as the baseline to compare brain response during mental stimulus and during rest period [50]. Many studies have been done on transcranial Doppler outcomes obtained from envelope signals which are peak velocity signals extracted from raw signals [51]. They did not consider findings from raw signals [52], [53], [54]. Raw signals and envelope signals may show distinct cerebral blood flow characteristics which may demonstrate the significance of extraction of envelope signals and preservation of raw signals. More supplementary information might be provided by considering raw signals. In this way, we examined both raw signals and the spectral envelope signals.

In our study, we analyzed many characteristics to characterize SCI brain response. Our major contributions include the understanding of signal characteristics in time domain, fre-

quency domain and in time-frequency domain. Techniques for extracting the set of features are explained in the third chapter. Furthermore, we tried to understand the brain organization and the hemispheric functioning investigating the extracted features. Finally, these signal characteristics were then compared to CBFV in healthy participants and participants with other neurological disorders. The last chapter summarizes our outcomes and the possible direction of future work. Following these objectives, we will be able to better understand the effects of cervical SCI on brain response during rest periods and during cognitive stimuli.

2.0 BACKGROUND

2.1 SPINAL CORD INJURY

2.1.1 Spinal Cord

The spinal cord is a set of nervous tissue enclosed in the bony spinal column [55]. The spinal cord is a fundamental part of the central nervous system which also includes the brain [56]. Nerve fibers make up the cerebral cord that extends from the brain. The spinal cord receives information from body tissues and from the brain. Then, the spine relays this information between the brain and peripheral nervous system through cerebral fibers in the form of electrical signals. The second function of spinal cord serves as the basis for reflexes: it contains neural circuits which control reflexes (independently of the brain and the rest of the central nervous system) [55], [57].

The spinal cord is a flexible column whose origin is situated in the foramen magnum (the opening in the occipital bone of the skull) [56]. The length of the spinal cord is much shorter than the length of the bony spinal column, approximately 25 cm shorter [58], [59]. In fact, the spine is continuous on the upper two thirds of the vertebral canal until the conus medullaris. This part of the spine is located in the space between the first and second lumbar vertebrae of the spinal column. The lumbar and sacral spinal nerves have long roots that extend below the last segment of spinal cord [56]. In fact, the last part of the vertebral canal called the filum terminale is filled with these spinal nerve roots and meninges. The dural sac ends at the vertebral level of the second sacral vertebra [58], [59].

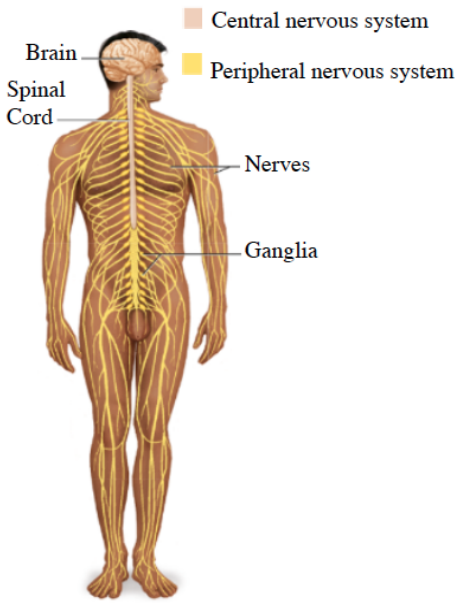

Figure 2: Central and peripheral nervous systems; adapted from Saladin [60]

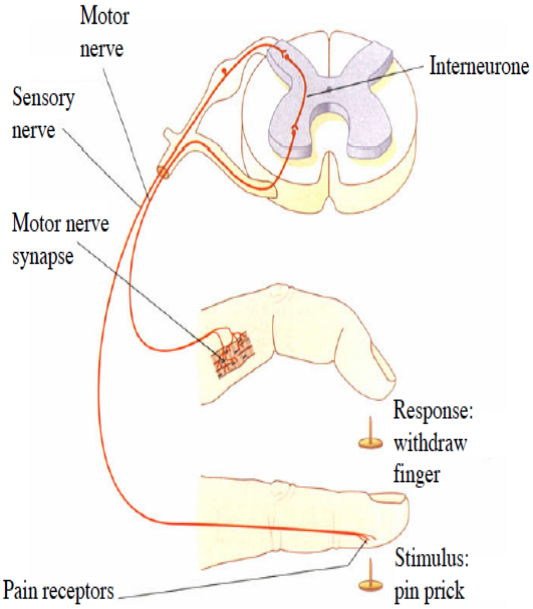

Figure 3: Reflex functioning; adapted from Sheerin [57]

The vertebral column serves as bony protection along the spinal cord. Indeed, other protective levels exist. Three layers of tissue known as spinal meninges surround the spinal cord. The dura mater is the peripheral protective layer and forms with the vertebral column the epidural space. It contains a network of vessels and fatty tissue. The intermediate arachnoid mater and pia matter are the innermost protective layers. The subarachnoid space is the space between these coatings which is filled by cerebrospinal fluid. The spinal cord is maintained on each side by denticulate ligaments. These stabilizing ligaments extend from the pia mater, cross the subarachnoid space and attach to the dura mater [57], [61], [62].

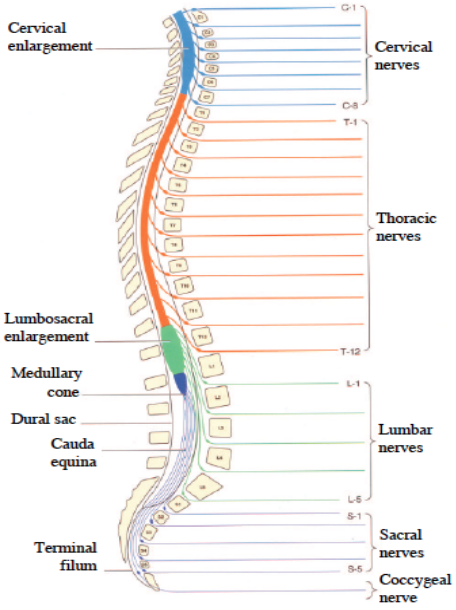

Figure 4: Spinal cord and bony spinal column; adapted from Gruener [63]

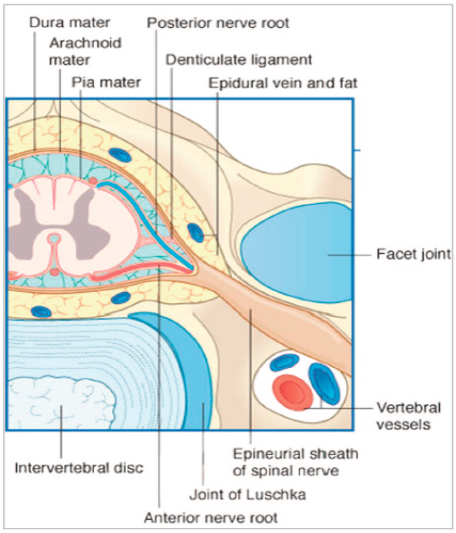

Figure 5: Spinal cord and protective layers; adapted from Sheerin [57]

The spinal cord has a cylindrical shape that is compressed on the dorsal and ventral sides. A cross-section of spinal cord shows two distinct regions: the white matter and the "H" or butterfly-shaped grey matter. The peripheral region of the spinal cord contains white matter while the internal region comprises the grey matter. The white matter consists of cerebral cells, sensory/motor neurons and their unmyelinated axons. On the opposite hand, the grey matter includes nerve cell bodies of interneurons and motor neurons, i.e. axons, dendrites and cell bodies [57], [64]. Grey and white matters surround the central canal of the spinal cord which is filled with cerebrospinal fluid. The central canal is an extension of cerebrospinal fluid cavities, i.e. brain ventricles [65].

2.1.2 Spinal Cord segments

The spinal cord is separated into 31 levels. The spinal cord is not "divided" into segments because the spinal cord is continuous on the upper two thirds of the vertebral canal. In fact, the segmentation comes from the segmentation of the vertebral column into 30 vertebrae. It

is also based on the vertebral origin of spinal nerves. The human spinal cord is split into 8 cervical segments, 12 thoracic segments, 5 lumbar segments, 5 sacral segments, 1 coccygeal segment [57], [66]. At every segment, pairs of right and left spinal nerves come out of the central nervous system. It contains mixed spinal nerves, i.e. sensory and motor nerves [66]. Indeed, sensory nerve rootlets on the dorsal side and motor nerve rootlets on the ventral side combine together to form nerve roots. Then, right/left motor and sensory roots join to form spinal nerves on the two sides of the spinal cord [63]. Rootlets/roots/spinal nerves are part of the peripheral nervous system. Concerning the sensory neurons, dorsal roots are combined to their corresponding pair of dorsal root ganglia. Cell bodies of sensory neurons are brought together in these ganglia even though their axons correspond with dorsal roots. Concerning the motor neurons, cell bodies are located in grey matter whereas ventral roots consist of their axons [64].

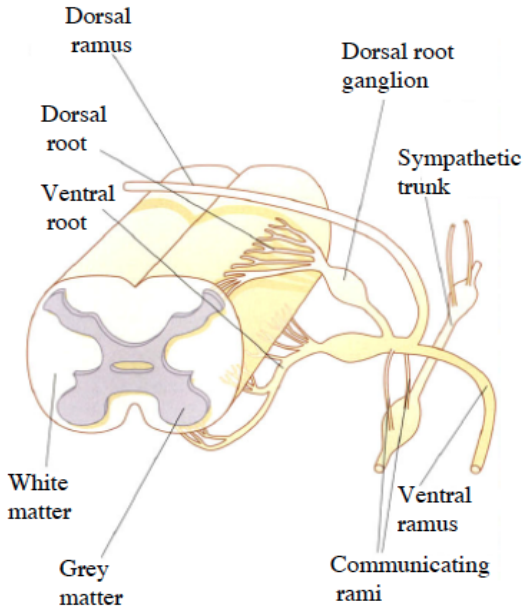

Figure 6: A cross-section of spinal cord and spinal nerve; adapted from Sheerin [57]

In the upper part of the spinal cord, spinal nerves exit directly at the level of the corresponding vertebra, while in the lower part, nerves go along the spinal cord before exiting.

The lowest segment nerves form a bunch of nerves to constitute the filum terminale or the cauda equina. Two spinal cord enlargements gather sensory and motor nerves that innervate the arms and the legs (cervical and lumbosacral enlargements respectively) [64].

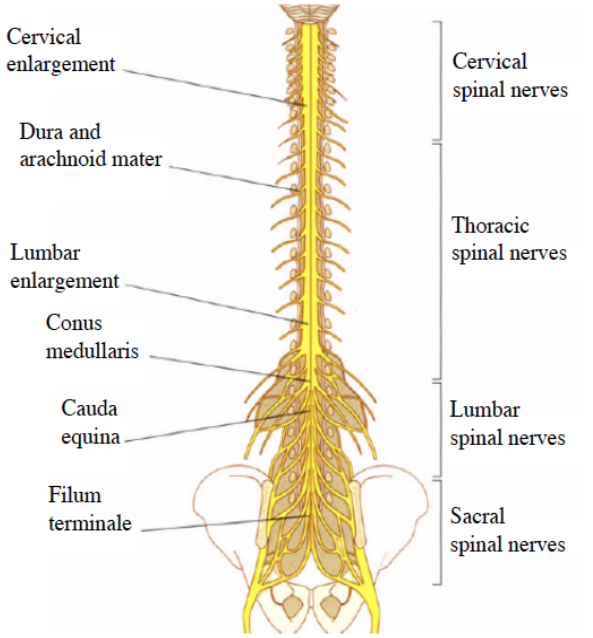

Figure 7: Enlargements in the lower and the upper sides of the spinal cord; adapted from Sheerin [57]

2.1.3 Spinal Cord Injury and symptoms

A spinal cord injury (SCI) corresponds with any injury to the spinal cord that is caused by trauma or by disease. A spinal cord injury in patients usually implies partial or full motor/sensory dysfunction [39] [40]. In fact, the symptoms can vary widely depending on the SCI location, ranging from "incomplete" SCI to "complete" SCI. "Incomplete" SCI is equivalent to few effects or no effect on functions whereas "complete" SCI shows total loss of functions [67], [68]. SCI may have repercussions on motor/sensory functions below the injury in the spinal cord either for complete or for incomplete lesions. Sensory modification may lead to numbness, pain and a loss of sensation while motor control may be disrupted by

motor alteration (uncontrollable or unresponsive contraction and weakness) [69]. Cervical injuries lead to full or partial tetraplegia/ quadriplegia. Thoracic lesions result in paraplegia while the lumbosacral SCI may cause problems on lower limb control, sexual, bladder and rectum functions [68], [70]. The most recent report from the US National SCI Statistical Center revealed that cervical SCI represents 54% of cases, 36% of SCI cases correspond to thoracic SCI and 10% SCI are correlated to lumbosacral SCI [71].

In addition, the SCI level is designated by the lesion location on the spinal column. Defining the level of SCI remains a crucial point for determining the exact consequences of SCI. In fact, cervical spinal cord lesion on the third vertebra and on the fifth vertebra lead to different preservation/loss of functions [68], [70]. Table 2 summarizes the potential loss of motor/sensory abilities.

Table 2: Level of injury and their corresponding consequences on human body; adapted from Health Encyclopedia of University of Rochester- Medical Center [69]

Level of injury	Motor/sensory repercussions
C2-C3	Quadriplegia and inability to breathe
C4	Quadriplegia and difficulty to breathe
C5	Quadriplegia with some elbow and shoulder functions
C6	Quadriplegia with some elbow, wrist and shoulder functions
C7	Quadriplegia with some elbow, wrist, hand and shoulder functions
C8	Quadriplegia with normal arm functions and hand weakness
T1-T6	Paraplegia with loss of function below the mid-chest
T6-T12	Paraplegia with loss of function below the waist
L1-L5	Paraplegia with some loss of functions in legs (a wide range of degree)

These contributions showed that SCI can lead to other health disorders: cardiovascular and broncho-pulmonary diseases, musculoskeletal, gastro-intestinal, renal and immune dysfunctions in addition to incomplete/complete tetraplegia/paraplegia and dysfunctions [43], [72].

2.1.4 Classification, causes and Spinal Cord Injury Recovery

Following an SCI, physicians perfom clinical examinations of strength and sensation to classify the exact level of SCI. This examination gathers a clinical test of myotome and a clinical test of dermatome. A section of skin innervated through a definite part of the spine is called a dermatome while a group of muscles innervated through a definite part of the spine is called a myotome. The American Spinal Injury Association (ASIA) first published an international classification of spinal cord injury in 1982, called the International Standards for Neurological and Functional Classification of Spinal Cord Injury. Nowadays, in its sixth edition, the degree of motor/sensation loss is determined according to the neurological examination. 10 key muscles' strength and sensory function on 28 dermatomes are tested bilaterally in the upper limb and in the lower limb based on the International Standards for Neurological and Functional Classification of Spinal Cord Injury [67], [73], [74]. In fact, dermatomes are tested by light touch and pinprick. Myotomes are graded (including elbow flexors, wrist flexors, elbow extensors, finger flexors, small finger abductors, hip flexors, knee extensors, ankle dorsiflexors, long toe extensors, ankle plantarflexors). [69]

The severity of SCI is evaluated according to the American Spinal Injury Association Impairment Scale (AIS). It can be described by 5 levels of loss function where A is a complete loss of muscle control and sensory function, B is a complete loss of motor activity and limited sensation in the sacral dermatomes, C or D is an incomplete loss of motor depending on the motor strength and E represents normal conditions [40], [75], [76].

The causes of spinal cord lesions are usually traumatic because of motor vehicle accidents, violence, falls and sport accidents [68]. SCI can be caused by non-traumatic lesions such as cancer, infection, disk degeneration, arthritis, inflammation [77]. Accidents may sever the spinal cord or the cauda equina or may cause swelling and rupturing of the coating of the nerve fibers. More than 80% of SCI patients are men and more than 50% of SCI subjects are patients between 16 and 30 years old [68], [78].

The SCI recovery mainly depends on the severity of the lesion. Entire rehabilitation from complete injuries is usually rare while recovery from incomplete lesions may be conceivable. However, determining the exact outcomes after an SCI is a real challenge. In fact, the motor

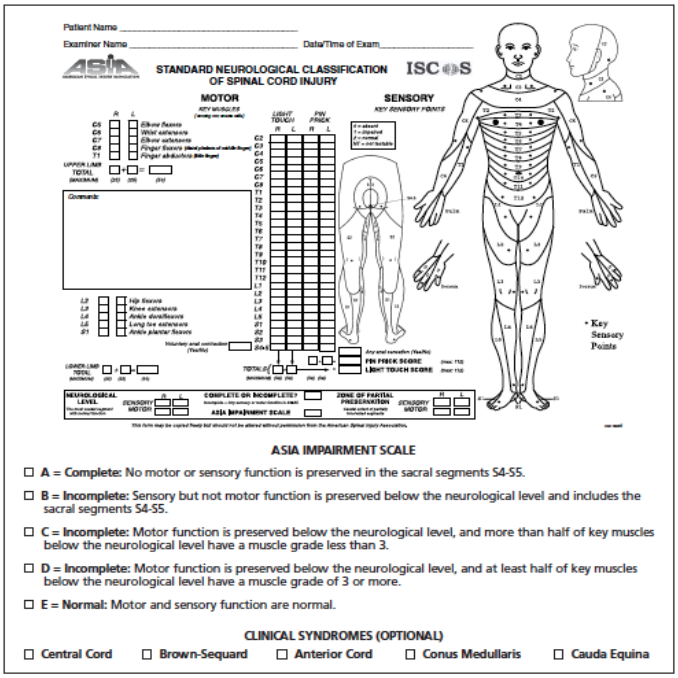

Figure 8: Spinal cord examination following lesion; adapted from Wing [73]

and sensory effects of SCI can vary in a wide range [69]. Most SCI patients gain one level of motor function in the first 6 months to possibly a few years after lesion. For instance, 86% of incomplete SCI ASIA C-D subjects regain motor function while only 3% of patients with SCI classified as complete ASIA A turn into incomplete ASIA D [79]. Additionally, other parameters are included in rehabilitation: level of the SCI, type of motor and sensory impairements and age and general physical condition [69].

Initial medical care following an SCI has considerably improved in the past few years. First, the spinal cord is stabilized following SCI during transport and resuscitation. Second, surgical care is widespread with the aim of limiting paralysis. Indeed, decompressing the spine means removing bone, disc or ligament fragments. Surgical interventions may yield improvements after an SCI but most lesions are permanent. Pharmacological treatments are also used to reduce spine inflammation and pression such as steroid methylprednisolone [79].

2.2 INSONATED CEREBRAL ARTERIES

2.2.1 Main cerebral arteries

TCD is mainly used to target main cerebral arteries [80]. Usually, transducers are placed on the thinnest parts of the head bone which are the acoustic windows of the skull allowing us to monitor activities on cerebral arteries of the circle of Willis. The transtemporal window enables us to reach the middle (MCA), anterior (ACA) and posterior (PCA) cerebral arteries. The transforaminal window enables us to reach the basilar and the vertebral arteries; while the transorbital window enables us to reach the ophthalmic and the internal arteries [81].

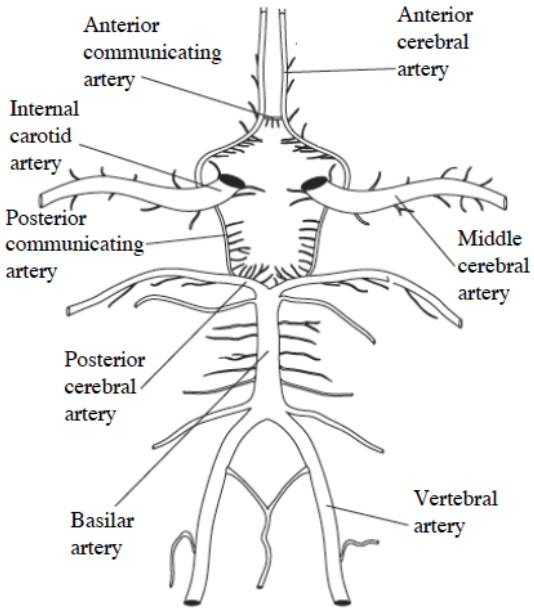

Figure 9: Cerebral arteries and circle of Willis; adapted from Alastruey [82]

Arteries are identified by understanding the depth of insonation, the transducers position and the flow direction [83]. Table 3 summarizes criteria to determine cerebral arteries.

The most commonly insonated arteries are the ACA, the MCA and the PCA [84]. Each of these arteries supplies blood to different areas: the ACA supply to the medial regions, the MCA supply to the lateral regions and the PCA supply to the posterior basomedial regions.

Table 3: Identification of cerebral arteries (CA); adapted from White [81]

Artery	Window	Flow direction	Depth in mm	Velocity in cm/s
Middle CA	Temporal	Toward	35-60	46-86
Anterior CA	Temporal	Away	60-75	41-76
Posterior CA	Temporal	Toward	60-75	33-64
Orbital CA	Orbital	Toward	40-50	16-26
Vertebral CA	Foraminal	Away	45-75	27-55
Basilar CA	Foraminal	Away	70-120	30-57

2.2.2 Middle cerebral arteries

The MCA is most usually insonated in studies about cognitive processes [24], [85], [86], [87], as 80% of blood to the brain is delivered by the MCA. Moreover, MCA is usually easier to detect in contrast with other cerebral arteries due to brain anatomical structure [81]. In this way, MCA study appears to be judicious in understanding brain response during resting-state and activation periods.

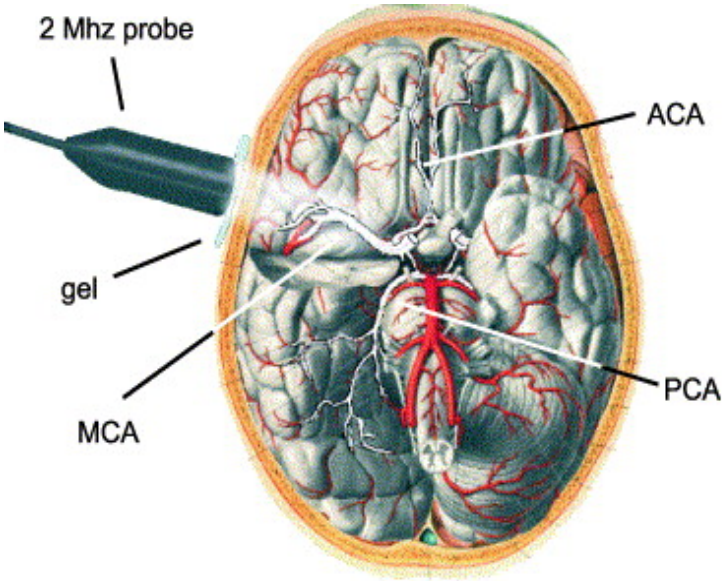

Figure 10: Measurement of cerebral blood flow on MCA; adapted from Sheerin [3]

2.3 COLLECTING CEREBRAL BLOOD FLOW VELOCITY SIGNALS WITH TRANSCRANIAL DOPPLER

2.3.1 Idealized cerebral blood flow

TCD measures CBFV making a hypothesis about the distribution of cerebral velocity. In fact, the arterial blood flow velocity is characterized by a parabolic speed profile which can be described by the following function $v(r)$ [3]:

$$v(r) = \frac{R_0^2 - r^2}{4\eta} \frac{\Delta p}{l} \tag{2.1}$$

where r is the distance to the arterial symmetry axis (where $r = 0$), η corresponds to the blood viscosity, Δp represents the pressure gradient along an arterial distance l.

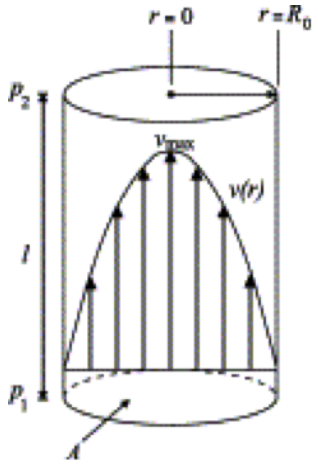

Figure 11: Idealized cerebral blood flow velocity distribution; adapted from Deppe [3]

The maximum velocity into distribution is located in the center of the artery where $r = 0$. Envelope signals are usually extracted from raw signals, which are a sum of signals corresponding to erythrocytes' movement at different velocities. v_{max} is described by the following formula [3]:

$$v_{max} = \frac{R_0^2 \Delta p}{4\eta l} \tag{2.2}$$

where R_0 is related to the arterial cross-section A. Indeed, v_{max} is correlated to the entire cross-section where $A = \pi R_0^2$. v_{max} is usually called a spectral envelope signals [3].

2.3.2 Doppler effect

TCD is based on the Doppler effect thanks to emission of ultrasounds. A transducer, which is at the same time the transmitter and the receiver, sends an ultrasound which has a frequency superior to 2 MHz [88]. This wave comes into contact with erythrocytes in the blood stream of the artery. It is reflected to the transducer because of the red blood cell movement and their speed. It causes a modification of the frequency of ultrasound which can be calculated by spectral estimation. The cerebral blood flow can be calculated thanks to the difference between the produced wave and the reflected wave. Frequency variation is due to wavelength variation which depends on the distance crossed by erythrocytes during the wave's period [89].

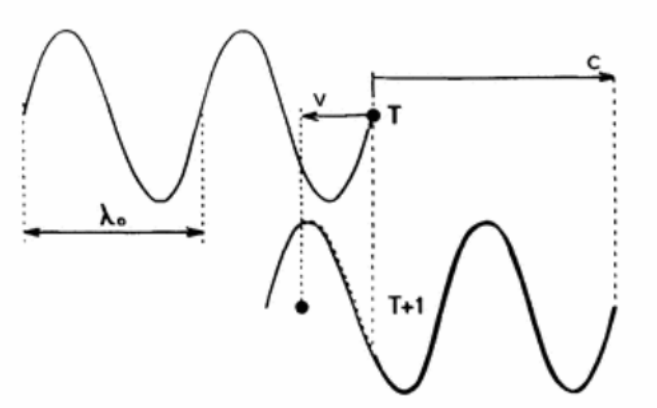

Figure 12: Doppler effect; adapted from Aaslid [20]

To have valid results, the knowledge of insonation angle is essential [3], [81].

$$v = \frac{c\Delta f}{2cos\theta f} \tag{2.3}$$

where θ is the insonation angle, v the erythrocytes' speed, f the ultrasound frequency of the emitted signal, c the ultrasound speed and Δf the frequency shift between the produced and the reflected signals.

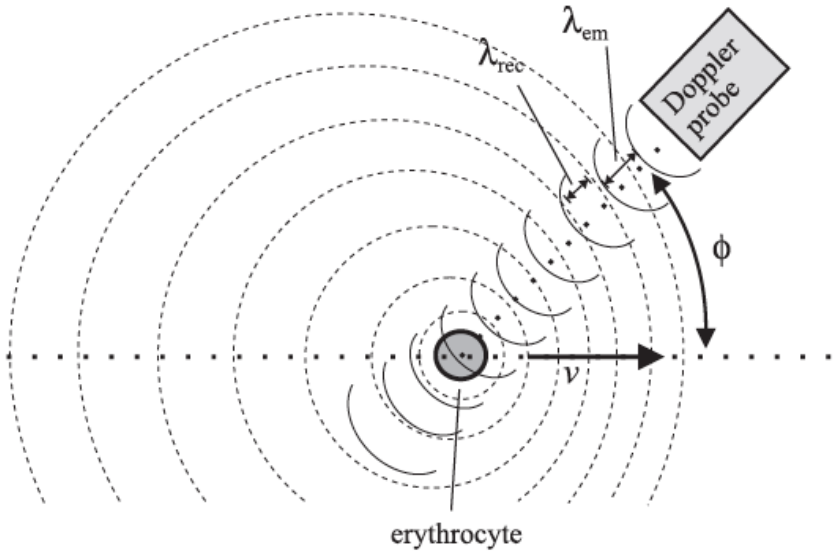

Figure 13: Doppler effect and angle of insonation; adapted from Deppe [3]

Previously, only one blood cell was considered. Indeed, ultrasounds are reflected by a large number of erythrocytes. Many reflections contribute to the detected signal which correspond to a sum of sinusoidal signals [3]:

$$s(t) = \sum_{i=0}^{n} a_i s_i(f_i, t) = \sum_{i=0}^{n} a_i sin(2\pi f_i t + \phi_i) \tag{2.4}$$

where a_i are weighting factors and ϕ_i represent the phase of the signal at $t = 0$.

Actually, Fast Fourier transform was initially used in the Doppler system. Nevertheless, the error rate was found to be high for a low number of periods. Now, the Doppler system measures velocity using the quadrature demodulation technique which presents a high time resolution. The number of misclassifications is independent of the number of signal periods. Figure 14 resumes the quadrature demodulation technique. A quadrature signal pair is generated as a sine and cosine signal pair or as a complex analytical signal with an electrical phase shifter on the original signal of constant frequency [90].

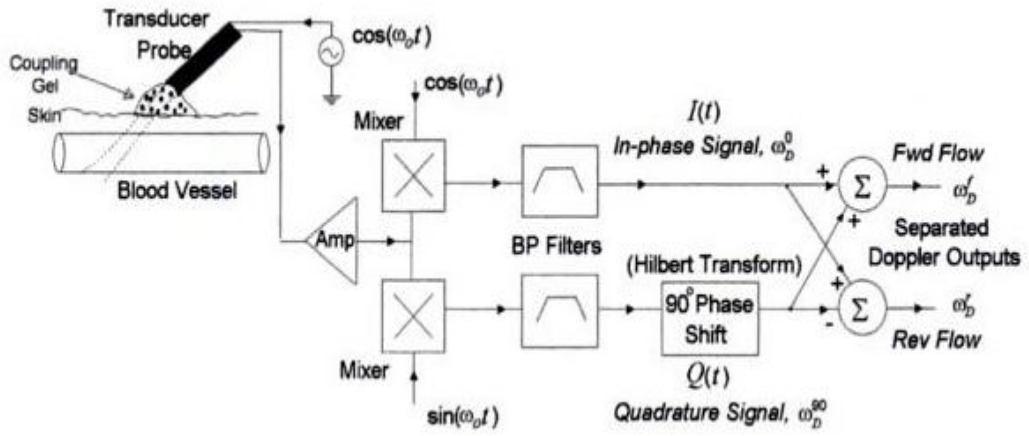

Figure 14: Doppler system using quadrature demodulation and Hilbert transform; adapted from Cobbold [91]

We consider that the original signal (received by the transducer) is $Ae^{j2\pi f_d t}$. This signal is mixed with in-phase and quadrature version of $cos(2\pi f_o t)$ where f_o and f_d represent the original frequency and the received frequency respectively. It gives the following outputs [92]:

$$I(t) = Ae^{j2\pi f_d t} cos(2\pi f_o t) \tag{2.5}$$

$$Q(t) = Ae^{j2\pi f_d t} sin(2\pi f_o t) \tag{2.6}$$

The signals $I(t)$ and $Q(t)$ represent the real and the imaginary parts of the desired Doppler signal $S(t) = I(t) + jQ(t)$ [92], [93]. The sum or the difference of these signals give the signals for flow toward and away from the transducer where [94]:

$$I(t) + jQ(t) = Ae^{j2\pi t(f_d + f_o)} \tag{2.7}$$

$$I(t) - jQ(t) = Ae^{j2\pi t(f_d - f_o)} \tag{2.8}$$

Since adding low-pass filters, the component $(f_d + f_o)$ is removed [94]. Then, the phase difference of the original and the received signals $(f_d - f_o)$ is determined with a polar coordinate transformation and an incremental period count which is achieved by detecting the 2π phase jumps. Finally, the instant Doppler frequency is calculated based on the phase difference using the equation (2.3) [90]. We also can use the Hilbert transformation to generate a quadrature signal pair. It is not really recommended because it does not anticipate the directional discrimination [90].

$$y(t) = H[x(t)] = \frac{1}{\pi} \int_{-\infty}^{+\infty} \frac{x(\tau)}{t - \tau} d\tau \tag{2.9}$$

The signal $y(t)$ results from the passing of $x(t)$ through the filter H following [95]:

$$H(t) = -jsgn(t) \tag{2.10}$$

In fact, the phase of the input signal rotates by $\frac{\pi}{2}$ or $-\frac{\pi}{2}$ depending on the function $sgn(t)$. The original signal is added to the resulting signal. We obtain the same signal as $I(t) - jQ(t)$ multiplying the sum of signals by $e^{-j2\pi f_o t}$, i.e. $e^{j2\pi t(f_d - f_o)}$. As with the quadrature demodulation technique, the erythrocytes' velocities are calculated based on $(f_d - f_o)$ [96].

In addition, the Doppler effect also provides the opportunity to calculate the depth of insonation which is a main point in arterial identification. The emitted ultrasound wave travels twice the distance between erythrocytes and the transducer following the relation [97]:

$$2d = c\Delta t \tag{2.11}$$

where Δt represents the time of ultrasound path, d is the depth of insonation and c is the ultrasound speed.

2.3.3 Collected signals

In this thesis, raw CBFV signals were collected using TCD. Raw signals comprise the various velocities of blood particles in cerebral arteries. In fact, signals are composed of several sinusoidal signals due to parabolic speed CBFV distribution [3]. We also considered the

maximal CBFV or envelope signals which corresponds to the maximal Doppler shift [3], [98]. Figure 15 and figure 16 give an example of raw and envelope signals along multiple heart periods of envelope signals.

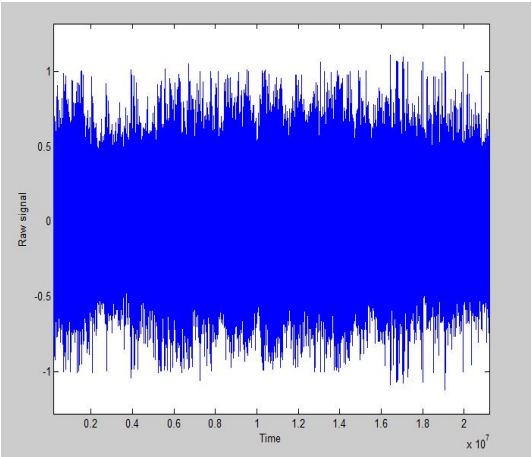

Figure 15: A raw signal extracted from a healthy participant signals from the right MCA

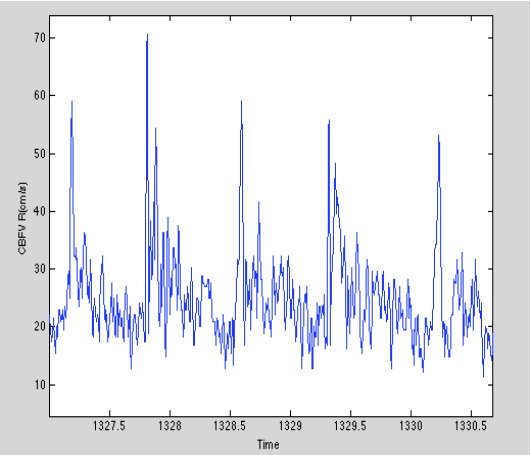

Figure 16: An envelope signal extracted from a healthy participant signals from the right MCA

2.4 SPINAL CORD INJURIES AND COGNITIVE BRAIN RESPONSE

SCI implied an impairment of supraspinal regulation of autonomic function. This deterioration entailed hypotension and sudden peaks of hypertension [43], [99]. An impaired tension control affects the response of cerebral blood flow and brain metabolic demands during mental or physical challenges. In fact, the maintenance of sufficient cerebral blood flow is based on arterial baroreflex and cerebral autoregulation. The cerebral autoregulation adapts cerebral blood flow depending on the brain needs while the arterial baroreflex maintains the arterial blood pressure. Consequently, the brain response to cognitive processes could be impacted by the dysfunctional tension control which involves a reduction of focus, memory or reasoning [47], [48], [49], [100]. Only a few TCD studies examined CBFV in SCI patients during mental tasks. These studies showed that CBFV through MCA from participants with SCI above the sixth thoracic segment does not increase during cognitive tests (attention and verbal tests). This indicates a deficient cognitive performance due to hypotension [46]. Nevertheless, CBFV from SCI subjects is constantly lower than CBFV from non-SCI subjects during resting-state periods [46]. However, other TCD studies established clearly the connection between hypotension and an impaired cerebral blood flow during mental activities [84], [101], [102]. Subjects with hypotension show a reduced CBFV and less distinct CBFV increase during stimulus cognitive activities than healthy subjects [103].

3.0 METHODOLOGY

3.1 CASE STUDY

This is a case study of CBFV in a single participant with SCI. The participant's SCI is at the level of the fifth cervical vertebra. The subject had no history of heart murmurs, strokes, concussions, migraines or other brain-related injuries. The participant was asked to sign the consent form approved by the University of Pittsburgh Institutional Review Board.

3.2 PROCEDURE

The MCA signals were collected with a SONARA TCD System (Carefusion, San Diego, CA, USA). Two 2 MHz transducers were fixed with a headset on the two sides of the skull. They were placed on transtemporal windows (5 cm in front of the ears, above the zygomatic arch [104]) to reach MCA signals. MCA were identified depending on the depth of insonation (45-55 mm), the angle of insonation (perpendicularly to the skull) and the flow direction (towards transducers) [81], [83]. Additionally, the end-tidal carbon dioxide $ETCO_2$ (BCI Capnocheck Sleep Capnograph, Smiths Medical, Waukesha, Wisconsin, USA) was monitored along with respiration rate, electrocardiogram, head movement and skin conductance via a multisystem physiological data monitoring system (Nexus-X, Mindmedia, Netherlands). After the acquisition of R-ACA and L-ACA cerebral blood flow data in the form of audio files, raw signals were extracted with a sampling frequency of 44100Hz. Information was downsampled by a factor 5 (8820 Hz) to accelerate computation.

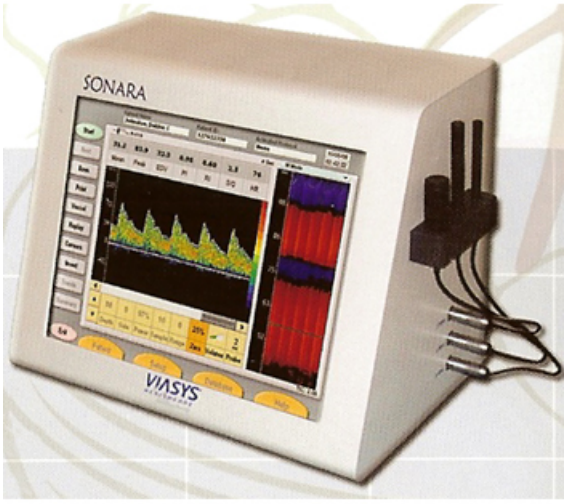

Figure 17: MCA measurement on TCD System

The participant was asked to complete 20 minutes of resting-state followed by two 15-minute periods of cognitive processes. During the 20 minutes of resting state, the subject was requested to sit motionless and maintain a thought-free mental state. The 15-minute parts of mental tasks were separated by a 5-minute break. However, we did not collect data during these five minutes. Each 15-minute block comprises 5 word generation tasks, 5 mental rotation tasks and 5 resting conditions of 45 seconds between each cognitive task. During geometric tasks, pairs of images were randomly selected from a database constructed from 3-D cubes and were displayed. The subject was requested to rotate displayed models to define connections between pairs of images (mirror symmetrical or identical). During the word generation task, letters which were randomly chosen were displayed at the beginning of each period. The participant generated words based on these letters. A non-verbal mode of answering was chosen to avoid activation of brain regions associated with speech. In each mental block, the order of tasks was randomly chosen.

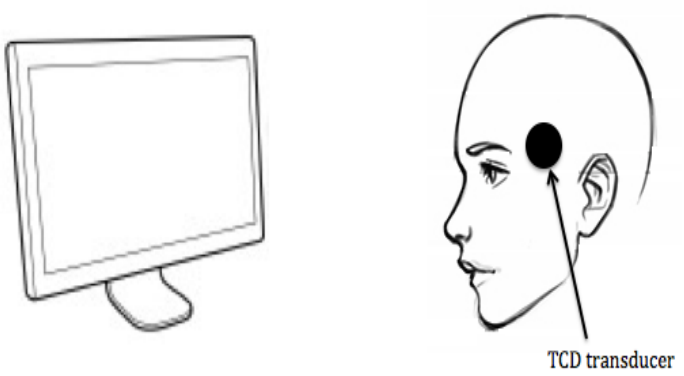

Figure 18: Setup for the study

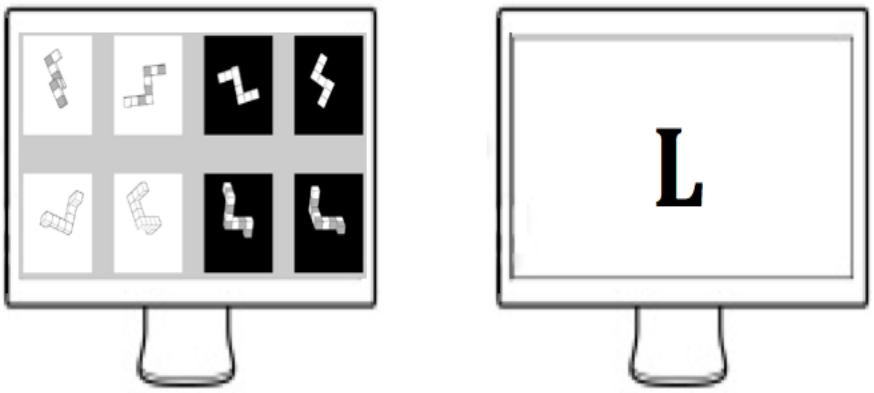

Figure 19: An on-screen sample of geometric and word-generation tasks

3.3 FEATURE EXTRACTION

3.3.1 Time features

MCA signals on the right side and on the left side were characterized by the second, the third and the fourth moments, i.e. standard deviation, skewness and kurtosis of the signal

[105], [106]. Standard deviation of the amplitude distribution represents the dispersion of data from the average of a distribution [105], [107]:

$$\sigma = \sqrt{\frac{1}{n-1}\sum_{i=1}^{n}(x_i - \mu)^2} \tag{3.1}$$

where μ denotes the mean value of the signal X.

The skewness of a signal evaluates the asymmetry of the distribution [105], [108]:

$$\epsilon = \frac{\frac{1}{n}\sum_{i=1}^{n}(x_i - \mu)^3}{(\frac{1}{n}\sum_{i=1}^{n}(x_i - \mu)^2)^{\frac{3}{2}}} \tag{3.2}$$

The kurtosis of a distribution describes the shape of the distribution around tails [105], [109]:

$$\gamma = \frac{\frac{1}{n}\sum_{i=1}^{n}(x_i - \mu)^4}{(\frac{1}{n}\sum_{i=1}^{n}(x_i - \mu)^2)^2} \tag{3.3}$$

The cross-correlation coefficient at the zero lag measure the similarity between two signals (right MCA and left MCA):

$$CC_{X/Y} = \frac{1}{N}\sum_{i=1}^{N}(x_i y_i) \tag{3.4}$$

where the signal X and Y represent signals from the right and the left side of the MCA [110].

3.3.2 Information-theoretic features

The Lempel-Ziv complexity (LZC) measures the randomness, the predictability and the regularity of discrete-time signals [111]. It is widely used in biomedical applications, specially to study brain activities [112], [113]. The signal data is transformed into finite sequences. 99 thresholds are defined to divide the signal into 100 finite spaces T_h, $1 \leq h \leq 99$, $h \in \mathbb{Z}^+$ [114]. Then, parts of the quantized signal $X_1^n = \{x_1, x_2, \cdots, x_n\}$ are gathered to shape blocks [115]:

$$B = X_j^l = \{x_j, x_{j+1}, \cdots, x_l\}, 1 \leq j \leq l \leq n, j, l \in Z^+ \tag{3.5}$$

where each block has length L defined by $j - l + 1$ and represents a series of successive data. For each L, every block is analyzed. A counter c is defined to illustrate the amount of

new pattern formation. It increases by one unit if the sequence of a block has not already appeared in previous analysis. Finally, the LZC was given as the following formula where the final c measures the complexity of the signal and n represents the total of quantized levels in the signal:

$$LZC = \frac{c(log_{100}c + 1)}{n} \tag{3.6}$$

The entropy rate ρ of a stochastic process measures the statistic degree of recurrence of patterns of a signal for medical data analysis [116]. The normalized pattern distribution (zero mean and unit variance) is quantized into 10 equal levels. Then, the distribution $X = \{x_1, x_2, \cdots, x_n\}$ is decomposed and grouped into blocks of length L, $10 \leq L \leq 30$. A block L represents a finite sequence of successive samples in the quantized distribution such as $\Omega_L = \{\omega_1, \omega_2, \cdots, \omega_{n-L+1}\}$ [117].

$$\omega_i = 10^{L-1}x_{i+L-1} + 10^{L-2}x_{i+L-2} + \cdots + 10^0 x_i \tag{3.7}$$

where ω_i is classified between 0 and $10^L - 1$. The Shannon entropy $S(L)$ defined the degree of complexity of ω_L given the quantized signal Ω_L where X takes discrete values ω_j with probability p_j [117]:

$$S(L) = \sum_{j=0}^{10^{L-1}} p_j ln p_j \tag{3.8}$$

where p_j is the approximated sample joint probability of the pattern j in Ω_L with the understanding that $\sum_{j=1}^{n-L+1} p_j = 1$ with $0 \leq p_j \leq 1$ $i = 1, \cdots, n - L + 1$. The normalized conditional entropy was defined as [118]:

$$N(L) = \frac{S(L) - S(L-1) + S(1)pe(L)}{S(1)} \tag{3.9}$$

where $pe(L)$ is the percentage of patterns with length L that appeared only once in ω_L. $S(1)$ is the conditional entropy estimation of the stochastic process for $L = 1$ and represents the Shannon entropy of white noise. It is multiplied by the same probability distribution $pe(L)$. Thus, $S(1)pe(L)$ is a corrective term added due to the underestimation of $S(L) - S(L-1)$ for larger L [119]. Given that the first term decreases while the second term increases with L, the function $N(L)$ shows a minimum $min(N(L))$ which is the best estimation of the conditional

entropy. $min(N(L))$ is an index of complexity. Conversely, $\rho = 1 - min(N(L))$ is an index of regularity whose values vary between 0 and 1 [118].

Two probability functions can be compared thanks to the cross-entropy rate. It quantifies the mutual information between two distributions. It predicts data in a signal from previous and current information in an other signal. The two X and Y were normalized, quantized and computed according to the conditional entropy method. Finally, the cross-entropy rate $\Omega_L^{X|Y}$ (information rate available in one of the samples of the quantized signal X when a pattern of $L-1$ samples of the quantized signal Y) was computed as [118]:

$$\omega_i^{X|Y} = 10^{L-1}x_{i+L-1} + 10^{L-2}y_{i+L-2} + \cdots + 10^0 y_i \tag{3.10}$$

The normalized cross-entropy was established as:

$$NC_{X|Y}(L) = \frac{S_{X|Y}(L) - S_Y(L-1) + S_X(1)pe_{X|Y}(L)}{S_X(1)} \tag{3.11}$$

where $S_X(L)$, $S_Y(L)$ and $S_{X|Y}$ represent the Shannon entropies of the distribution X, Y and $\Omega_L^{X|Y}$. $pe_{X|Y}(L)$ is the percentage of patterns with length L that appeared only once in $\omega_L^{X|Y}$ and $S_X(1)pe_{X|Y}(L)$ is a corrective term added due to the underestimation of $S_{X|Y}(L) - S_Y(L-1)$ for larger L. As with the previous method, $S_X(1)$ is the conditional entropy estimation of the stochastic process X for $L = 1$. The Shannon entropy of white noise $S_X(1)$ is multiplied by the same probability distribution $pe_{X|Y}(L)$. The previous function exhibits a minimum $min(NC_{X|Y}(L), NC_{Y|X}(L))$. The index of synchronization $\Lambda_{X|Y} = 1 - min(NC_{X|Y}(L), NC_{Y|X}(L))$ varies between 0 (X and Y are independent processes) and 1 (X and Y are synchronized).

3.3.3 Frequency features

Frequency features were also extracted. The discrete Fourier transform (DFT) entails the projection of the observed signal from time domain to frequency domain. The sequence of uniformly spaced N samples of the observed signal is considered where x_n is a complex number [120].

$$X_k = \sum x_n e^{\frac{-j2\pi kn}{N}} \tag{3.12}$$

where k is an integer and X_k is a vector of N complex numbers. N is the period of the observed signal x_n. In fact, we assumed that collected signals were periodic.

The peak frequency, the centroid frequency and the bandwidth of the spectrum were examined to identify the spectral characteritics of the signal [121],[122]. The peak frequency is defined as the maximal spectral power:

$$f_p = arg_f max\{|F_X(f)|^2\} \tag{3.13}$$

where $F_X(f)$ is the Fourier transform of the signal X and f_{max} in this study was 8820 Hz. The spectral centroid is computed as the center of mass of the spectrum [123]:

$$f_c = \frac{\int_0^{f_{max}} f|F_X(f)|^2 \, \mathrm{d}f}{\int_0^{f_{max}} |F_X(f)|^2 \, \mathrm{d}f} \tag{3.14}$$

The bandwidth of the spectrum represents the squared differences between the spectral centroid and the spectral components [121]:

$$B = \sqrt{\frac{\int_0^{f_{max}} (f - f_c)^2 |F_X(f)|^2 \mathrm{d}f}{\int_0^{f_{max}} |F_X(f)|^2 \mathrm{d}f}} \tag{3.15}$$

3.3.4 Time-frequency domain

The Fourier transform signal or spectrum signal can be performed in many problems. However, the frequencies of one signal may evolve over time in few cases. In fact, time-frequency domain allows us to observe the time-evolution of the frequencies and exhibits the signal dynamics.

To avoid aliasing, window size could be used. Nevertheless, the window size is fixed. Another method in analyzing frequency content called the wavelet transform enables variable window sizes. These varied windows are obtained from the scaling (dilation and contraction) and from shifting. The wavelet transform of a signal $x(t)$ can be found as below [124]:

$$wt(s,\tau) = \frac{1}{\sqrt{s}} \int_{-\infty}^{\infty} x(t)\psi^*(\frac{t-\tau}{s})dt \tag{3.16}$$

where $s > 0$ is the scaling parameter, τ is the shifting parameter and $\psi * (.)$ represents the complex conjugation of the base wavelet $\psi(t)$. s and τ may vary continously in the case of continuous wavelet transform.

Using the continuous wavelet transform may lead to redundant data. In that case, discrete wavelet transform and translation parameters may be performed to reduce the computational time as the following equation: $s = s_0^j$ and $\tau = k\tau_0 s_0^j$ where $s_0 < 1$, $\tau_0 \neq 0$ and $j, k \in Z$. Usually, $s_0 = 2$ and $\tau_0 = 1$ [124].

The base wavelet is obtained as [124]:

$$\psi_{j,k}(t) = \frac{1}{\sqrt{2^j}}\psi(\frac{t-k2^j}{2^j}) \tag{3.17}$$

Therefore, the wavelet transform of a signal x(t) is calculated as:

$$wt(j,k) = \frac{1}{\sqrt{2^j}} \int_{-\infty}^{\infty} x(t)\psi^*(\frac{t-k2^j}{2^j})dt \tag{3.18}$$

$\psi_{j,k} = 2^{-i/2}\psi(2^{-j}t - k)$ is considered as a collection of orthogonal bases. Then, for a given signal $x(t)$ where J is a predetermined scale [124]:

$$x(t) = \sum_{j=-\infty}^{J} \sum_{k=-\infty}^{\infty} d_{j,k}\psi_{j,k}(t) + \sum_{k=-\infty}^{\infty} a_{J,k}\psi j, k(t) \tag{3.19}$$

When the predetermined scale J goes to ∞:

$$x(t) = \sum_{j=-\infty}^{\infty} \sum_{k=-\infty}^{\infty} d_{j,k}\psi_{j,k}(t) \tag{3.20}$$

The scale function $\phi(t)$ and wavelet function $\psi(t)$ can be described as below [124]:

$$\phi(t) = \sum_{n} h(n)\phi_{-1,n}(t) = \sqrt{2}\sum_{n} h(n)\phi(2t-n) \tag{3.21}$$

$$\psi(t) = \sum_{n} g(n)\phi_{-1,n}(t) = \sqrt{2}\sum_{n} g(n)\phi(2t-n) \tag{3.22}$$

where $h(n)$ and $g(n)$ are a low-pass and a high-pass wavelet filters respectively.

Following the Mallat algorithm, $x(t)$ can be expressed as [124]:

$$x(t) = \sum_{k} a_{j-1,k}2^{(-j+1)/2}\phi(2^{-j+1}t-k) = \sum_{k} a_{j,k}2^{-j/2}\phi(2^{-j}t-k) + \sum_{k} d_{j,k}2^{-j/2}\psi(2^{-j}t-k) \tag{3.23}$$

where $a_{j,k} = \sum_m h(m-2k)a_{j-1,m}$ and $d_{j,k} = \sum_m h(m-2k)d_{j-1,m}$.

The signal $x(t)$ goes through low-pass and high-pass filters. It is decomposed into low-frequency components ($a_{j,k}$) and high-frequency components ($d_{j,k}$). The different coefficients at wavelet decomposition level j are obtained by applying low and high pass filters to the approximate coefficients $a_{j-1,k}$ at the previous decomposition level $(j-1)$ [124], [125].

The Meyer wavelet is an orthogonal and symmetric function. In the frequency domain [124], [125]:

$$\psi(f) = \begin{cases} \sqrt{2\pi}e^{i\pi f}sin(\frac{\pi}{2}v(3|f|-1)) & \text{if } 1/3 \le |f| \le 2/3 \\ = \sqrt{2\pi}e^{i\pi f}cos(\frac{\pi}{2}v((3/2)|f|-1)) & \text{if } 2/3 \le |f| \le 4/3 \\ = 0 \qquad \text{otherwise} \end{cases} \tag{3.24}$$

where $v(\alpha) = \alpha^4(35 - 84\alpha + 70\alpha^2 - 20\alpha^3)$ and $0 \le \alpha \le 1$

Based on a 10-level discrete wavelet decomposition of the signal using the discrete Meyer wavelet, the signal is decomposed into 10 levels $W = [a_{10}\ d_{10}\ d_9\ \cdots\ d_1]$ where a_{10} is the approximation coefficient and d_k represents detail coefficients at the k^{th}-level [126]. The signal is observed at various frequency bands and various positions. Then, the relative wavelet energy from the approximation coefficients is defined by the following formula [127]:

$$\Xi_a = \frac{\|a_{10}\|^2}{\|a_{10}\|^2 + \sum_{k=1}^{10} \|d_k\|^2}(\%) \tag{3.25}$$

$$\Xi_{d_k} = \frac{\|d_k\|^2}{\|a_{10}\|^2 + \sum_{k=1}^{10} \|d_k\|^2}(\%) \tag{3.26}$$

where $\|.\|$ is the Euclidian norm. The relative wavelet energy defined the relative energies within different frequency bands depending on the ratio between the k-th level of decomposition and the total energy of the signal.

A wavelet entropy Ω measures the degree of order/disorder of the signal [127]. It represents the concentration of wavelet energies on the band of levels:

$$\Omega = -\Xi_{a_{10}} log_2 \Xi_{a_{10}} - \sum_{k=1}^{10} \Xi_{d_k} log_2 \Xi_{d_k} \tag{3.27}$$

where Ξ is the relative energy calculated above in 3.25 and in 3.26.

3.3.5 Comparisons and statistical test

The non-parametric statistical hypothesis Wilcoxon rank-sum test was used to compare statistical differences between results. Wilcoxon rank sum statistic tests the equality of the marginal distributions (not necessarily Gaussian distributions) when sampling from two populations. This test is proposed to identify sets of data from the same distribution. This method is based on ranks of the original observations. Two unpaired groups of data $X = [x_1, x_2, \cdots, x_n]$ and $Y = [y_1, y_2, \cdots, y_m]$ were extracted from the left side and the right side of MCA where n and m are the sample sizes of the two groups respectively. Let L and R be the distribution functions corresponding to the two samples. Independence between the two samples was assumed and the null hypothesis is H_o: "no difference between the

two groups" or $R(t) = L(t)$ for every time t. The two-sided alternative is H_1: "there is a difference between R and L" or $R(t) > L(t)/R(t) < L(t)$.

The first step is combining all the values from each group in ascending order. The smallest number gets a rank of 1 and the largest number gets a rank $N = n + m$.

Table 4 and table 5 below show the combined data associated with the rank. In table 4, we assume that the two populations have distinct values. So, all the ranks are distinct. In table 5, we assume that y_8 and x_5 have the same value.

Table 4: Ranked combined data of two distributions L and R (all the ranks are distinct)

Data	x_3	y_8	x_5	x_1	y_6	$\cdots$	y_1
Rank	1	2	3	4	5	$\cdots$	$n+m$

Table 5: Ranked combined data of two distributions L and R (the two groups share a few similar values)

Data	x_3	y_8	x_5	x_1	y_6	$\cdots$	y_1
Rank	1	2.5	2.5	4	5	$\cdots$	$n+m$

We assumed that the two groups have distributions with the same shape. Then, the rank median in each group is calculated. If the median of the two groups are very different, the p-value will be small and the null hypothesis is rejected. The two groups are distinct. On the opposite side, if it is similar, the p-value will be high and the null hypothesis is not rejected. It doesn't mean that the two populations are the same.

The observed rank sum W associated with the first group R is calculated.

$$W = \sum_{i=0}^{n} rank(R)_i \tag{3.28}$$

All the possible permutations of the ranks into which m ranks are assigned to group R and n ranks are assigned to group L are calculated. For each permutation, we found the rank sum for population R. The number of rank sum S is defined.

The p-value is determined following the below equations (p_{upper} in the upper tail and p_{lower} in the lower tail) [128], [129]:

$$p_{upper} = \frac{P(S \leq W)}{\binom{m+n}{n}} \tag{3.29}$$

$$p_{lower} = \frac{P(S \geq W)}{\binom{m+n}{n}} \tag{3.30}$$

In our study, we examined the effects of the mental task, the geometric task and the resting-state period. $p < 0.05$ indicates statistical significance of the extracted features [130].

4.0 RESULTS

The end-tidal carbon dioxide level does not influence the mean diameter of the middle cerebral arteries [13]. Consequently, it is not taken into consideration. Secondly, the results are presented in tables in the form of ($mean \pm standard\ deviation$) where the rest period is pointed out by an "R", the verbal task is indicated by a "V" and a "G" shows the geometric tasks. R-MCA indicates the right MCA, while L-MCA indicates the left MCA.

4.1 TIME FEATURES

Table 6 summarizes time-domain feature values for the raw and the envelope signals. For raw CBFV signals, a few statistical differences were detected. The standard deviation in R-MCA decreased during the cognitive tasks ($p < 0.05$), while it was larger during the geometric tasks than during the word-generation tasks ($p = 0.04$). Furthermore, statistical differences were noticed between resting-state periods and mental processes on the kurtosis value on the left-sided signals ($p < 0.05$). The kurtosis is higher during cognitive challenges than during baseline periods (particularly during word-generation tasks). While considering the features on the envelope signals, a lower correlation value was noticed during verbal tasks than during the resting-state periods ($p = 0.05$).

Table 6: Time features from raw and envelope CBFV signals (* denotes multiplication by 10^{-3}, † denotes multiplication by 10^{-7}). CBFV are in units of centimeters per second.

		RAW		ENVELOPE	
		R-MCA	L-MCA	R-MCA	L-MCA
Mean CBFV	R	$(10.7 \pm 6.94)^{\dagger}$	$(-4.45 \pm 3.56)^{\dagger}$	38.0 ± 8.68	36.6 ± 5.41
	V	$(1.12 \pm 7.00)^{\dagger}$	$(0.18 \pm 6.67)^{\dagger}$	37.2 ± 6.25	36.0 ± 4.96
	G	$(3.13 \pm 8.18)^{\dagger}$	$(0.89 \pm 6.51)^{\dagger}$	33.0 ± 6.06	33.3 ± 4.79
Standard Deviation	R	0.14 ± 0.01	0.12 ± 0.01	9.18 ± 2.39	9.89 ± 2.51
	V	0.10 ± 0.02	0.10 ± 0.02	15.8 ± 4.41	15.0 ± 5.23
	G	0.12 ± 0.01	0.12 ± 0.01	12.6 ± 3.96	11.3 ± 3.07
Skewness	R	$(-1.11 \pm 0.71)^{*}$	$(-2.03 \pm 4.44)^{*}$	1.01 ± 0.50	0.96 ± 0.15
	V	$(0.39 \pm 5.51)^{*}$	$(0.52 \pm 6.70)^{*}$	1.47 ± 0.45	1.40 ± 0.47
	G	$(0.91 \pm 2.87)^{*}$	$(-0.39 \pm 5.60)^{*}$	1.80 ± 0.62	1.60 ± 0.56
Kurtosis	R	3.11 ± 0.04	$3.09 \pm (3.92)^{*}$	4.76 ± 2.13	4.07 ± 0.59
	V	3.40 ± 0.19	3.37 ± 0.22	5.84 ± 2.49	5.45 ± 1.86
	G	3.28 ± 0.23	3.28 ± 0.18	7.76 ± 3.30	6.90 ± 2.71
Cross-Correlation	R	$(15.0 \pm 1.97)^{*}$		0.97 ± 0.01	
	V	$(13.7 \pm 1.50)^{*}$		0.88 ± 0.06	
	G	$(14.2 \pm 1.89)^{*}$		0.91 ± 0.06	

4.2 INFORMATION-THEORETIC FEATURES

Information-theoretic features from both CBFV raw and CBFV envelope signals are presented in table 7. For the envelope signals, the entropy rate was higher during the geometric-rotation periods in R-MCA than in L-MCA ($p = 0.05$).

Table 7: Information-theoretic features from raw and envelope CBFV signals (* denotes multiplication by 10^{-3}).

		RAW		ENVELOPE	
		R-MCA	L-MCA	R-MCA	L-MCA
LZC	R	0.68 ± 0.01	0.69 ± 0.01	0.66 ± 0.05	0.68 ± 0.04
	V	0.68 ± 0.02	0.68 ± 0.01	0.66 ± 0.04	0.67 ± 0.03
	G	0.68 ± 0.02	0.67 ± 0.01	0.63 ± 0.04	0.66 ± 0.04
Entropy rate	R	0.41 ± 0.10	0.34 ± 0.10	0.04 ± 0.03	$(3.69 \pm 1.62)^*$
	V	0.37 ± 0.10	0.41 ± 0.07	0.07 ± 0.07	0.04 ± 0.05
	G	0.42 ± 0.11	0.44 ± 0.09	0.12 ± 0.09	0.06 ± 0.06
Index synchronization	R	0.35 ± 0.08		0.12 ± 0.04	
	V	0.36 ± 0.08		0.12 ± 0.06	
	G	0.38 ± 0.10		0.16 ± 0.13	

4.3 FREQUENCY FEATURES

Table 8 summarizes the frequency characteristics of raw and envelope signals. For raw signals, the peak frequency was higher during geometric-rotation tasks than during verbal processes in L-MCA ($p = 0.05$). Additionally, a statistical difference on the peak frequency was observed between R-MCA and L-MCA during word-generation tasks. The peak frequency of R-MCA was higher ($p = 0.02$). The bandwidth values of R-MCA signals increased during cognitive processes ($p < 0.05$). The bandwidth was larger during the verbal tasks than during the geometric-rotation periods ($p = 0.04$). For envelope signals, a small increase of the R-MCA bandwidth was noticed during the verbal processes in comparison to the resting-states ($p = 0.03$). In addition, larger peak frequency in L-MCA signals was observed during geometric-rotation periods than during verbal challenges ($p = 0.01$).

A rise of peak frequency was observed on the R-MCA between mental processes (higher during geometric processes than during word-generation tasks). However, the p-value is not significant enough on the right side to be considered ($p = 0.2$).

Table 8: Frequency features from raw and envelope CBFV signals (* denotes a multiplication by 10^{-3}).

		RAW		ENVELOPE	
		R-MCA	L-MCA	R-MCA	L-MCA
Spectral Centroid	R	897 ± 149	898 ± 108	8.46 ± 1.84	13.2 ± 3.20
	V	923 ± 104	887 ± 69	15.3 ± 1.77	14.8 ± 2.35
	G	849 ± 105	842 ± 75	13.9 ± 3.25	14.4 ± 1.71
Peak frequency	R	644 ± 170	600 ± 90.5	1.56 ± 0.97	1.76 ± 0.77
	V	764 ± 579	446 ± 54.9	0.54 ± 0.88	0.62 ± 0.81
	G	732 ± 595	884 ± 755	1.25 ± 1.08	1.84 ± 0.80
Bandwidth	R	495 ± 26.7	554 ± 53.5	12.1 ± 0.75	13.6 ± 1.17
	V	636 ± 65.8	615 ± 80.3	14.4 ± 0.30	14.3 ± 0.50
	G	579 ± 54.8	565 ± 46.3	13.8 ± 0.90	14.1 ± 0.38

4.4 TIME-FREQUENCY FEATURES

Table 9 shows the wavelet entropy values for raw and envelope signals. The wavelet entropy values for raw signals increased during the verbal processes in comparison to other periods on the right side of CBFV signals ($p < 0.05$). As raw signals, statistical differences between baseline periods and cognitive processes were highlighted on the two sides of CBFV envelope signals ($p < 0.03$). An increase of wavelet entropy was observed on R-MCA and L-MCA signals. Each side of MCA showed an increase of wavelet energy which is larger during verbal processes than during other periods.

Table 9: Wavelet entropy values for raw and envelope CBFV signals (* denotes multiplication by 10^{-3}).

		RAW		ENVELOPE	
		R-MCA	L-MCA	R-MCA	L-MCA
	R	1.60 ± 0.06	1.73 ± 0.10	$0.04 \pm (0.54)^*$	$0.05 \pm (5.68)^*$
Ω	V	1.81 ± 0.10	1.83 ± 0.12	0.13 ± 0.06	0.13 ± 0.07
	G	1.71 ± 0.08	1.75 ± 0.07	0.11 ± 0.05	0.10 ± 0.05

Figures 20 and 21 present the feature values of wavelet energy decomposition on the raw and the envelope signals. The relative energy of a raw CBFV signal was mainly concentrated in d_{10}, d_9, d_8 and d_7, while the relative energy of the envelope signal concentrated in a_{10} during all periods. The relative energy of R-MCA raw signals in d_{10} increased during cognitive processes ($p < 0.05$), while diminishing in d_8 during the geometric-rotation processes ($p = 0.03$). The concentration on the level a_{10} from envelope signals remained relatively stable (with a slight decrease) between baseline results and cognitive processes on the two sides of MCA ($p = 0.03$).

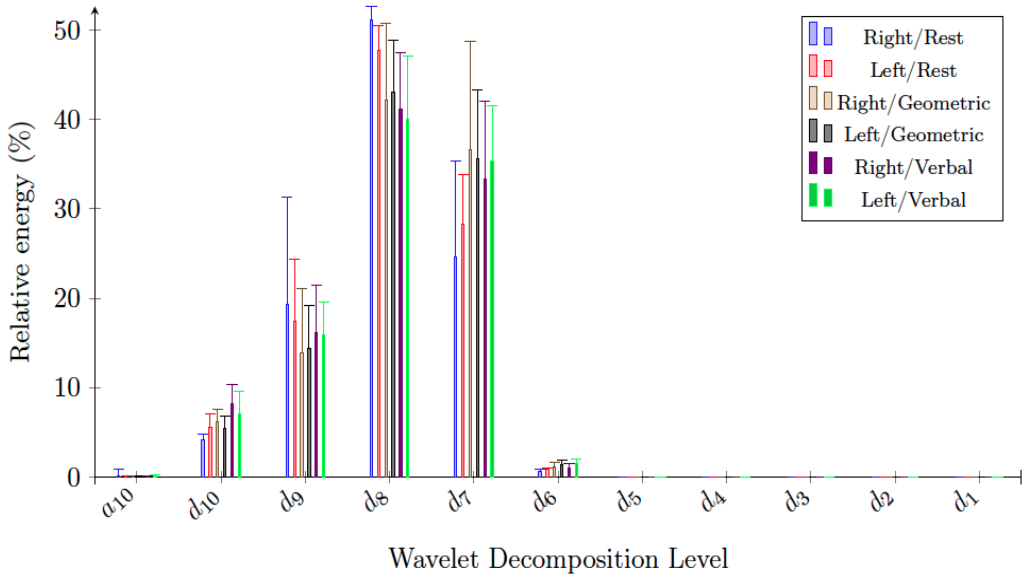

Figure 20: The 10 level wavelet decomposition of raw signals

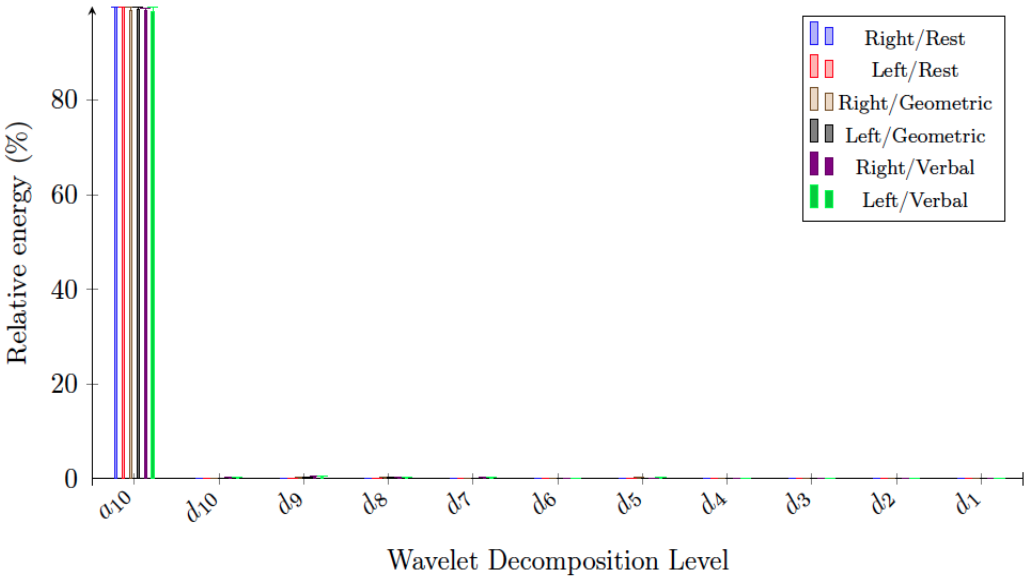

Figure 21: The 10 level wavelet decomposition of envelope signals

5.0 DISCUSSION

5.1 MCA SIGNALS

Each domain (time, information-theoretic, frequency and time-frequency domains) revealed the effects of cognitive tasks on CBFV in R-MCA and L-MCA demonstrating the consequences and the repercussions of a spinal cord injury at a cervical level.

The probability density function shapes of R-MCA and L-MCA signals were examined based on the analysis of time domain components. Raw R-MCA signals exhibited small standard deviation values during mental processes, particularly during word-generation periods. This demonstrated that CBFV signals were more concentrated around the mean of probability density function during cognitive challenges. In fact, it proved that the cerebral blood flow changed in a wider range in the case of geometric processes than in the case of word-generation tasks. Changes in kurtosis values for raw L-MCA signals between the resting-state and the cognitive tasks were also noticed. The rise of kurtosis is higher during word-generation tasks than during geometric-rotation challenges. First, it proved that the CBFV variations on the left side of MCA were different depending on the cognitive task type. Second, kurtosis represents the distribution peakedness and flatness [131]. Higher kurtosis proved that the cerebral blood flow is massed around one value. Indeed, the left-sided raw signals were more dispersive during verbal challenges than during geometric tasks. Signals extracted during verbal tasks centralized information around one value because of lower right-sided standard deviation and higher left-sided kurtosis. During the word-generation periods, cross-correlation of envelope signals decreased comparing to the resting-state periods. In fact, a reduction of the cross-correlation values between the verbal tasks and the baseline underlined lower dependence between right-sided and left-sided signals. This implies lower

dependence on the functioning of the two hemispheres pointing out a lateralization which implies modifications of bilateral dependence between the two hemispheres. In this study, verbal processes may introduce a lateralization where one hemisphere is more engaged in cerebral blood perfusion.

In the information-theoretic domain, the L-MCA envelope signals exhibited lower entropy rates than R-MCA signals during geometric-rotation tasks, which proved that these signals were more random than right-sided signals. Additionally, a lower entropy highlighted a faster cerebral blood flow. In this way, CBFV is higher on the left side of MCA during geometric tasks. Finally, the information-theoretic domain revealed lateralization during the brain response while performing geometric tasks where left brain regions were more activated than right brain regions.

In frequency domain, the raw signals showed a band-pass profile while the envelope outcomes exhibited a low-pass structure. Furthermore, a noticeable increase of peak frequency in L-MCA and R-MCA raw signals revealed a stronger cerebral blood flow during geometric/verbal processes respectively. This increase in peak frequencies denotes a faster variation of cerebral blood flow velocity during cognitive challenges. It reinforced the previous statements about left lateralization during geometric-rotation periods (highlighted by the information-theoretic domain) and right lateralization during word-generation tasks (highlighted by the time-domain). Lastly, the bandwidth of R-MCA was larger during the cognitive tasks than during the resting-state indicating faster cerebral blood flow variations.

Lower wavelet entropy values demonstrated that raw and envelope signals were more ordered during rest periods than during cognitive challenges. In fact, time-frequency domain proved once again that mental processes led to variations of CBFV signals when compared to resting state. Furthermore, a very low wavelet entropy implies a very ordered signal which refers to a periodic mono-frequency signal in the case of envelope signals [127]. We noticed statistical differences on the raw and the envelope wavelet energy outcomes. Concerning the raw CBFV signals, a global increase of wavelet energy on d_{10} was noticed in the right side of MCA during mental challenges in contrast with baseline outcomes. The slight decrease of wavelet energy on a_{10} was also considered in both sides of MCA during cognitive processes from envelope results. Modifications of energy distribution exhibited modifications of CBFV

during cognitive tasks in the two sides of MCA. However, wavelet energy did not provide sufficient modifications to observe one lateralization during mental processes.

Finally, a dominance of one hemisphere was concluded during each cognitive task: pre-eminence of R-MCA/L-MCA during word-generation periods/geometric-rotation tasks. In fact, CBFV is higher in one side of the brain than in the other side depending on the type of cognitive process. However, only a few noticeable statistical differences proved lateralizations during mental tasks leading us to believe that brain lateralization in this patient is not as pronounced.

5.2 SPINAL CORD INJURY STUDY PARTICIPANT AND CONTROL SUBJECTS

Next, CBFV from able-bodied participants and the participant with cervical SCI were compared during each period. CBFV outcomes and brain response from healthy participants were extracted from different studies [52], [53], [98], [132]. This pointed out higher mean maximum velocities on MCA from control subjects (either during resting-state or during cognitive challenges). CBFV increased by 37% to 49% during each period between able-bodied participants and the SCI participant. A few studies also emphasized a lateralization of CBFV on MCA signals during mental processes from healthy participants. In fact, the geometric task should lead to a dominance of the left hemisphere (L-MCA) while the word-generation processes should lead to a dominance of the right hemisphere (R-MCA) from results on healthy participants [52], [53], [133], [134]. Outcomes from the participant affected by a cervical SCI turned out a similar slight lateralization during cognitive periods. The participant affected by a cervical SCI presented a "regular" brain lateralization during cognitive challenges which was couterbalanced by a low cerebral blood flow. Additionally, a brain functioning difference was observed between rest and mental processes. A CBFV decrease was discovered in the case of SCI subject while a CBFV rise was noticed in the case of control subjects during cognitive periods when compared to resting-state [52], [53].

5.3 SPINAL CORD INJURY AND NEUROLOGICAL DISORDERS

Then, results from the participant with SCI were compared to results from subjects affected by other "frequent" neurological disorders including Alzheimer's disease, autism, epilepsy, Parkinson's disease, and traumatic brain injury (TBI) [135]. A few studies examined effects of neurological disorders on CBFV outcomes during rest periods and/or mental challenges. In fact, this study was focused on neurological disorders which display few similarities to SCI results. Previously, we discovered that SCI outcomes revealed a "regular" brain lateralization during cognitive challenges, a decreased cerebral blood flow during each period (by 37% to 49%) and higher cerebral blood flow during resting-state. Low blood flow could be explained by impaired hypoperfusion and blood pressure in the case of SCI subject.

In a similar way to SCI results, several studies about Alzheimer's disease subjects revealed low CBFV during resting periods. It is reduced by 31% when compared to able-bodied participants [136], [137], [138]. Moreover, Alzheimer's disease subjects showed an altered brain response to mental activities during early states of the disease [136], [137], [138]. Similar to SCI neurological disorder, impaired brain response could be explained by hypoperfusion and modified blood pressure. Recent studies observed important blood pressure oscillations from Alzheimer's disease subjects which imply impaired autonomic function and a CBFV autoregulation [136]. Hypoperfusion in the case of Alzheimer's disease implies a lower cerebral blood demand during cognitive tasks and rest periods [137]. Nevertheless, brain lateralization is not equivalent to hemisphere dominance from SCI subject. Concerning Alzheimer's disease subjects, a few studies highlighted that left hemisphere is less involved in brain functioning during cognitive tasks than in SCI hemisphere functioning [139], [140]. One study pointed out a right-hemispheric dysfunction during mental processes [141].

Parkinson's disease participants revealed similar deficient brain response to SCI subject. Temporal and parietal areas showed lower cerebral blood flow in the case of Parkinson's disease patients with deficient cognitive response and/or dementia. In fact, these cerebral regions are supplied by MCA. Finally, local cerebral blood flow reduces by 10% during rest periods and during cognitive tasks in contrast with control subject CBFV [139], [142], [143]. Hypoperfusion is a cause of low CBFV in the case of Parkinson's disease exactly as it is the

origin of low CBFV in the case of SCI subjects. On the opposite side, Parkinson's disease subjects without impaired cognitive activity and dementia have regular CBFV on both sides of MCA [139], [144]. Additionally, Parkinson's disease subjects displayed high left-sided hypoperfusion. This underlined a general dominance of right hemisphere during each period [139].

Then, variations between autistic subjects CBFV and SCI participant CBFV were studied. In the case of autistic subjects, cerebral regions which are supplied by MCA (frontal, temporal and parietal brain regions) exhibited decreased general brain perfusion. A general perfusion decrease of 38% to 42% was detected [145], [146]. It would be difficult to compare autism brain function to SCI brain function because of autism diversity. Autistic cerebral response characteristic could be explained by brain atrophy, by anticonvulsants or by mental retardation while SCI impaired cognitive functions is explained by impaired blood pressure and tension [146], [147]. Then, autistic subjects without impaired cognitive activity may present normal brain lateralization during cognitive processes [148]. A few studies highlighted a general right hemisphere dominance in the case of autistic children with impaired cognitive activity [149], [150].

Regarding epilepsy, epilepsy seizures may imply CBFV decrease [151]. A few studies revealed decreased CBFV during abscence attacks (by 70%) due to hypotension and impaired autonomic function such as SCI [152], [153], [154]. Epilepsy attacks may cause cognitive deficits in attention, memory and speech [151]. This also demonstrated increased CBFV during severe epileptic seizures (by 160%) due to a rise of cerebral metabolism demand [152]. The CBFV demand increases because of fear, anxiety, memory activation [151]. Subjects may show regular or impaired lateralization [155], [156]. In one study, two thirds of the epileptic patients presented normal brain lateralization (left hemispheric dominance) and one third of the subjects presented abnormal hemisphere dominance (right-sided lateralization) during speech tasks [157].

Finally, traumatic brain injury (TBI) is deeply related to SCI. A TBI happens in 91% of traumatic SCI cases [46], [158]. This implies a decreased cerebral blood flow following injuries [159]. CBF decreases by 17% to 71% during the first twenty-four hours following the TBI and then, increases during the days following the TBI [160]. This phenomenon is due to an

intracranial pressure and a consecutive decrease in brain perfusion and in blood pressure. TBI patients usually present hypotension similar to SCI subject [161], [162]. One study revealed normal and abnormal brain lateralization during language tasks in the case of left hemispheric TBI. Right-handed participants exhibited regular left-sided hemisphere dominance while left-handed and mixed-handed subjects revealed impaired right-sided dominance [163].

Spinal cord injury, Alzheimer's disease, Parkinson's disease, autism and epilepsy present similarities such as decreased cerebral blood flow during resting-state periods/ during mental processes (except for epileptic subjects during seizures). However, the SCI participant pointed out low CBFV close to CBFV results from autistic subjects and Alzheimer's disease subjects. Regular brain lateralization appears as another point in common between SCI and other frequent neurological disorders in the case of: autistic subjects without impaired cognitive activity, epileptic patients in a few cases and TBI participants in a few cases.

6.0 CONCLUSIONS AND FUTURE WORK

6.1 CONCLUSIONS

In this thesis, we analyzed MCA cerebral blood flow velocity signals from a participant affected by a 5th cervical spinal cord injury during the resting-state, the word-generation tasks and the geometric-rotation tasks. Signals were characterized in time, frequency and time-frequency domains.

Time domain revealed changes in the two hemispheres' blood supplies between periods. The low cross-correlation on envelope signals between rest periods and word-generation processes emphasized low bilateral dependence between the hemispheres. Time, information-theoretic and frequency areas underlined a lateralization of MCA during the word-generation tasks/geometric-rotation processes which implied a stronger cerebral blood flow on one side of MCA (R-MCA/L-MCA). It is important to know that the lateralization conclusion about SCI participants is not perfectly clear. A few statistical differences do not point out a strong dominance of one hemisphere during cognitive tasks.

Comparison between outcomes from able-bodied subjects and a participant with SCI pointed out a "regular" brain lateralization during cognitive periods and a general decrease of CBFV on the two sides of MCA during each period in the case of SCI. However, higher CBFV was emphasized during rest periods from SCI outcomes which was a difference between control and SCI subjects.

Comparing SCI to other neurological disorders (Alzheimer's disease, autism, epilepsy, Parkinson's disease, and TBI) is a real challenge because of various neurological disorders' symptoms. Point of mutual interest is usually hypotension and deficient autonomic functions which implies impaired cognitive brain response. The SCI participant presented a noticeable

decrease of CBFV close to Alzheimer's disease subjects' and autistic patients' CBFV outcomes. Only autistic subjects without impaired cognitive activity, epileptic and TBI patients in a few cases presented the same normal brain lateralization to SCI participant.

6.2 FUTURE DIRECTIONS

Since the effects of SCI on cerebral blood flow have not been clearly studied, the research goal is to study the consequences of mental tasks on brain response and to compare outcomes to able-bodied control subjects. Our current project focuses on one SCI participant affected by a 5th cervical lesion. We characterized signals during three periods (resting-state and cognitive tasks) which should lead to different brain responses in the case of healthy subjects. Similar to control subjects, we discovered regular lateralization which differs by other aspects.

In the future, we might perform other sets of data collection with this participant to confirm the previous conclusion about brain response. However, since we want to design algorithms to distinguish cerebral blood flow response between SCI subjects and other participants (healthy or not), we may investigate data from other 5th cervical SCI subjects. Beyond these investigations, we will be able to extrapolate the understanding of brain response after this kind of SCI.

After these studies, we may try to identify cerebral blood flow outcomes from other cervical SCI and non cervical SCI. The goal might be the hemispheric characterization during regular left-sided and right-sided hemispheric brain response in the case of cervical, thoracic and lumbosacral lesions.

BIBLIOGRAPHY

[1] M. Demitri. (2014, May) Types of brain imaging techniques. [Online]. Available: http://psychcentral.com/lib/types-of-brain-imaging-techniques/0001057

[2] M. Raichle, "Behind the scenes of functional brain imaging: a historical and physiological perspective," *Proceedings of the National Academy of Sciences of the United States of America*, vol. 95, no. 3, pp. 765–772, 1998.

[3] M. Deppe, E. Ringelstein, and S. Knecht, "The investigation of functional brain lateralization by transcranial Doppler sonography," *Neuroimage*, vol. 21, no. 3, pp. 1124–1146, 2004.

[4] P. Fox and M. Raichle, "Focal physiological uncoupling of cerebral blood flow and oxidative metabolism during somatosensory stimulation in human subjects," *Proceedings of the National Academy of Sciences of the United States of America*, vol. 83, no. 4, pp. 1140–1144, 1986.

[5] M. Raichle and M. Mintun, "Brain work and brain imaging," *Annual Review of Neuroscience*, vol. 29, pp. 449–476, 2006.

[6] D. Attwell and C. Iadecola, "The neural basis of functional brain imaging signals," *Trends in Neurosciences*, vol. 25, no. 12, pp. 621–625, 2002.

[7] L. Pellerin and P. Magistretti, "Glutamate uptake into astrocytes stimulates aerobic glycosis: a mechanism coupling neuronal activity to glucose utilization," *Proceedings of the National Academy of Sciences of the United States of America*, vol. 91, no. 22, pp. 10 625–10 629, 1994.

[8] H. Forbes, "The cerebral circulation. I. Observation and measurement of pial vessels," *Archives of Neurology and Psychiatry*, vol. 19, no. 5, pp. 751–761, 1928.

[9] M. Raichle, "A brief history of human brain mapping," *Trends in Neurosciences*, vol. 32, no. 2, pp. 118–126, 2009.

[10] A. Aaslid, T. Markwalder, and H. Nornes, "Noninvasive transcranial Doppler ultrasound recording of flow velocity in basal cerebral arteries," *Journal of Neurosurgery*, vol. 57, no. 6, pp. 769–774, 1982.

[11] L. Brass, S. Pavlakis, and D. DeVivo, "Transcranial Doppler measurements of the middle cerebral artery. Effect of hematocrit." *Stroke*, vol. 19, no. 12, pp. 1466–1469, 1988.

[12] P. Huber and J. Handa, "Effect of contrast material, hypercapnia, hyperventilation, hypertonic glucose and papaverine on the diameter of the cerebral arteries. Angiographic determination in man," *Investigative Radiology*, vol. 2, no. 1, pp. 17–32, 1967.

[13] C. Giller, G. Bowman, H. Dyer, L. Mootz, and W. Krippner, "Cerebral arterial diameters during changes in blood pressure and carbon dioxide during craniotomy," *Neurosurgery*, vol. 32, no. 5, p. 737–742, 1993.

[14] H. Kontos, "Validity of cerebral arterial blood flow calculations from velocity measurements," *Stroke*, vol. 20, no. 1, pp. 1–3, 1989.

[15] M. Saqqur, K. Uchino, A. Demchuk, C. Molina, Z. Garami, S. Calleja, N. Akhtar, F. Orouk, A. Salam, A. Shuaib, and A. Alexandrov, "Site of arterial occlusion identified by transcranial Doppler predicts the response to intravenous thrombolysis for stroke," *Stroke*, vol. 38, no. 3, pp. 948–954, 2007.

[16] W. Burgin, M. Malkoff, R. Felberg, A. Demchuk, I. Christou, J. Grotta, and A. Alexandrov, "Transcranial Doppler ultrasound criteria for recanalization after thrombolysis for middle cerebral artery stroke," *Stroke*, vol. 31, no. 5, pp. 1128–1132, 2000.

[17] S. Knake, A. Haag, H. Hamer, C. Dittmer, S. Bien, W. Oertel, and F. Rosenow, "Language lateralization in patients with temporal lobe epilepsy: a comparison of functional transcranial Doppler sonography and the Wada test," *NeuroImage*, vol. 19, no. 3, pp. 1228–1232, 2003.

[18] C. Juhász, E. Scheidl, and I. Szirmai, "Reversible focal mri abnormalities due to status epilepticus. an eeg, single photon emission computed tomography, transcranial doppler follow-up study," *Electroencephalography and Clinical Neurophysiology*, vol. 107, no. 6, pp. 402–407, 1998.

[19] A. Whitehouse and D. Bishop, "Cerebral dominance for language function in adults with specific language impairment or autism," *Brain*, vol. 131, no. 12, pp. 3193–3200, 2008.

[20] R. Aaslid, *The Doppler principle applied to measurement of blood velocities in cerebral arteries*. Vienna: Springer, 1986.

[21] B. Conrad and J. Klingelhöfer, "Dynamics of regional cerebral blood flow for various visual stimuli," *Experimental Brain Research*, vol. 77, no. 2, pp. 437–441, 1989.

[22] J. Vollmer-Haase, K. Finke, W. Hartje, and M. Bulla-Hellwig, "Hemispheric dominance in the processing of J.S. Bach fugues: a transcranial Doppler sonography (TCD) study with musicians," *Neuropsychologia*, vol. 36, no. 9, pp. 857–867, 1998.

[23] S. Evers, J. Dannert, D. Rödding, G. Rötter, and E. Ringelstein, "The cerebral haemodynamics of music perception. a transcranial Doppler sonography study," *Brain*, vol. 122, no. 1, pp. 75–85, 1999.

[24] H. Markus and M. Boland, ""Cognitive Activity" monitored by non-invasive measurement of cerebral blood flow velocity and its application to the investigation of cerebral dominance," *Cortex*, vol. 28, no. 4, pp. 575–581, 1992.

[25] N. Stroobant, D. Buijs, and G. Vingerhoets, "Variation in brain lateralization during various language tasks: a functional transcranial Doppler study," *Behavioural Brain Research*, vol. 199, no. 2, pp. 190–196, 2009.

[26] R. Kelley, J. Chang, S. Suzuki, B. Levin, and Y. Reyes-Iglesias, "Selective increase in the right hemisphere transcranial Doppler velocity during a spatial task," *Cortex*, vol. 29, no. 1, pp. 45–52, 1993.

[27] C. Schnittger, S. Johannes, and T. Münte, "Transcranial Doppler assessment of cerebral blood flow velocity during visual spatial selective attention humans," *Neuroscience Letters*, vol. 214, no. 1, pp. 41–44, 1996.

[28] L. Cupini, M. Matteis, E. Troisi, M. Sabbadini, G. Bernardi, C. Caltagirone, and M. Silvestrini, "Bilateral simultaneous transcranial Doppler monitoring of flow velocity changes during visuospatial and verbal working memory tasks," *Brain*, vol. 119, no. 4, pp. 1249–1253, 1996.

[29] M. Silverstrini, C. Caltagirone, L. Cupini, M. Matteis, E. Troisi, and G. Bernardi, "Activation of healthy hemisphere in poststroke recovery. A transcranial Doppler study," *Stroke*, vol. 24, no. 11, pp. 1673–1677, 1993.

[30] F. Trabold, S. Meyer, P.G.and Blanot, and G. Carli, P.A.and Orliaguet, "The prognostic value of transcranial Doppler studies in children with moderate and severe head injury," *Intensive Care Medicine*, vol. 30, no. 1, pp. 108–112, 2004.

[31] B. Min, M. Marzelli, and S. Yoo, "Neuroimaging-based approaches in the brain-computer interface," *Trends in Biotechnology*, vol. 28, no. 11, pp. 552–560, 2010.

[32] M. Khalil, J. Tremoleda, T. Bayomy, and W. Gsell, "Molecular SPECT imaging: an overview," *International Journal of Molecular Imaging*, vol. 2011, no. Article ID 796025, pp. 1–15, 2011.

[33] M. Phelps, "PET: a biological imaging technique," *Neurochemical Research*, vol. 16, no. 9, pp. 929–940, 1991.

[34] J. Fiez, "Neuroimaging studies of speech. An overview of techniques and methodological approaches," *Journal of Communication Disorders*, vol. 34, no. 6, pp. 445–454, 2001.

[35] D. Thomas, E. Zilkha, S. Redmond, G. Du Boulay, J. Marshall, R. Ross Russell, and L. Symon, "An intravenous Xenon clearance technique for measuring cerebral blood flow," *Journal of the Neurological Sciences*, vol. 40, no. 1, pp. 53–63, 1979.

[36] E. Bernd Ringelstein, D. Droste, V. Babikian, D. Evans, D. Grosset, M. Kaps, H. Markus, D. Russell, and M. Siebler, "Consensus on microembolus detection by TCD," *Stroke*, vol. 29, no. 3, pp. 725–729, 1998.

[37] P. Schmidt, T. Krings, K. Willmes, F. Roessler, J. Reul, and A. Thron, "Determination of cognitive hemispheric lateralization by "functional" Transcranial Doppler cross-validated by functional MRI," *Stroke*, vol. 30, no. 5, pp. 939–945, 1999.

[38] W. Scott Burgin, M. Malkoff, R. Felberg, A. Demchuk, I. Christou, J. Grotta, and A. Alexandrov, "Transcranial Doppler ultrasound criteria for recanalization after thrombolysis for middle cerebral artery stroke," *Stroke*, vol. 31, no. 5, pp. 1128–1132, 2000.

[39] B. Cirak, S. Ziegfeld, V. Misra Knight, D. Chang, A. Avellino, and C. Paidas, "Spinal injuries in children," *Journal of Pediatric Surgery*, vol. 39, no. 4, pp. 607–612, 2004.

[40] C. Sadowsky, O. Volshteyn, L. Schultz, and J. McDonald, "Spinal-cord injury," *Disability and Rehabilitation*, vol. 24, no. 13, pp. 680–687, 2002.

[41] U. Parashari, S. Khanduri, S. Bhadury, N. Kohli, A. Parihar, R. Singh, N. Srivastava, and Upadhyay, "Diagnostic and prognostic role of MRI in spinal trauma, its comparison and correlation with clinical profile and neurological outcome, according to ASIA impairment scale," *Journal of Craniovertebral Junction and Spine*, vol. 2, no. 1, pp. 17–26, 2011.

[42] K. Kokotilo, J. Eng, and A. Curt, "Reorganization and preservation of motor control of the brain in spinal cord injury: a systematic review," *Journal of Neurotrauma*, vol. 26, no. 11, pp. 2113–2126, 2009.

[43] A. Phillips, P. Ainslie, A. Krassioukov, and D. Warburton, "Regulation of cerebral blood flow after spinal cord injury," *Journal of Neurotrauma*, vol. 30, pp. 1551–1563, 2013.

[44] A. Catz, V. Bluvshtein, A. Korczyn, I. Pinhas, I. Gelernter, T. Nissel, Y. Vered, N. Bornstein, and S. Akselrod, "Modified cold pressor test by cold application to the foot after spinal cord injury: suggestion of hemodynamics control by the spinal cord," *American Journal of Physical Medicine and Rehabilitation*, vol. 86, no. 11, pp. 875–882, 2007.

[45] S. Houtman, J. Serrador, W. Colier, D. Strijbos, K. Shoemaker, and M. Hopman, "Changes in cerebral oxygenation and blood flow during LBNP in spinal cord-injured individuals," *Journal of Applied Physiology*, vol. 91, no. 5, pp. 2199–2204, 2001.

[46] J. Wecht, D. Rosado-Rivera, A. Jegede, C. Cirnigliaro, M. Jensen, S. Kirshblum, and W. Bauman, "Systemic and cerebral hemodynamics during cognitive testing," *Clinical Autonomic Research*, vol. 22, no. 1, pp. 25–33, 2012.

[47] J. Morris, E. Roth, and G. Davidoff, "Mild closed head injury and cognitive deficits in spinal-cord-injured patients: incidence and impact." *Journal of Head Trauma Rehabilitation*, vol. 1, no. 2, pp. 31–42, 1986.

[48] Y. Tzeng, S. Lucas, G. Atkinson, C. Willie, and P. Ainslie, "Fundamental relationships between arterial baroflex sensitivity and dynamic cerebral autoregulation in humans," *Journal of Applied Physiology*, vol. 108, no. 5, pp. 1162–1168, 2010.

[49] G. Davidoff, E. Roth, P. Thomas, R. Doljanac, M. Dijkers, M. J. Berent, S., and G. Yarkony, "Depression and neuropsychological test performance in acute spinal cord injury patients: lack of correlation," *Archives of Clinical Neuropsychology*, vol. 5, no. 1, pp. 77–88, 1990.

[50] M. Fox and M. Raichle, "Spontaneous fluctuations in brain activity observed with functional magnetic resonance imaging," *Nature Reviews Neuroscience*, vol. 8, no. 9, p. 700, 2007.

[51] M. Deppe, S. Knecht, H. Henningsen, and E. Ringelstein, "Average: a Windows ®program for automated analysis of event related cerebral blood flow," *Journal of Neuroscience Methods*, vol. 75, no. 2, pp. 147–154, 1997.

[52] G. Vingerhoets and N. Stroobant, "Lateralization of cerebral blood flow velocity changes during cognitive task: a simultaneous bilateral transcranial Doppler study," *Stroke*, vol. 30, no. 10, pp. 2152–2158, 1999.

[53] R. Kelley, J. Chang, N. Scheinman, B. Levin, R. Duncan, and S. Lee, "Transcranial Doppler assessment of cerebral flow velocity during cognitive tasks," *Stroke*, vol. 23, no. 1, pp. 9–14, 1992.

[54] L. Lipsitz, S. Mukai, J. Hamner, M. Gagnon, and V. Babikian, "Dynamic regulation of middle cerebral artery blood flow velocity in aging and hypertension," *Stroke*, vol. 31, no. 8, pp. 1897–1903, 2000.

[55] M. Schwab, "Repairing the injured spinal cord," *Science*, vol. 295, no. 5557, pp. 1029–1031, 2002.

[56] R. Nieuwenhuys, J. Vooqd, and C. van Huijzen, *The human central nervous system: a synopsis and atlas.* Steinkopff, 4th edition, 2007.

[57] F. Sheerin, "Spinal cord injury: anatomy and physiology of the spinal cord," *Emergency Nurse*, vol. 12, no. 8, p. 30, 2004.

[58] J. Gianino, J. Paice, and M. York, *Intrathecal drug therapy for spasticity and pain.* Springer New York, 1996.

[59] S. Renowden, "Normal anatomy of the spinal cord," *Practical Neurology*, vol. 12, no. 6, pp. 367–370, 2012.

[60] K. Saladin, *Anatomy and physiology: the unit of form and function, 6th edition*. McGraw-Hill Science/Engineering/Math, 2010.

[61] D. Nicholas and R. Weller, "The fine anatomy of the human spinal meninges. A light and scanning electron microscopy study," *Journal of Neurosurgery*, vol. 69, no. 2, pp. 276–282, 1988.

[62] F. Vandenabeele, J. Creemers, and I. Lambrichts, "Ultrastructure of the human spinal arachnoid mater and dura mater," *Journal of Anatomy*, vol. 189, no. 2, pp. 417–430, 1996.

[63] G. Gruener and J. Biller, "Spinal cord anatomy, localization, and overview of spinal cord syndromes," *Continuum: Lifelong Learning in Neurology*, vol. 14, no. 3, pp. 11–35, 2008.

[64] H. Gray, *Anatomy of the human body*. Philadelphia: Lea and Febiger, 1918.

[65] K. Yasui, Y. Hashizume, M. Yoshida, T. Kameyama, and G. Sobue, "Age-related morphologoc changes of the central canal of the human spinal cord," *Acta Neuropathologica*, vol. 97, no. 3, pp. 253–259, 1999.

[66] S. Hochman, "Spinal cord," *Current Biology*, vol. 17, no. 22, pp. R950–R955, 2007.

[67] R. Waters, R. Adkins, and J. Yakura, "Definition of complete spinal cord injury," *Paraplegia*, vol. 29, pp. 573–581, 1991.

[68] O. Raineteau and M. Schwab, "Plasticity of motor systems after incomplete spinal cord injury," *Nature Reviews Neuroscience*, vol. 2, no. 4, p. 263, 2001.

[69] (2014, May) University of Rochester - Medical center - Health Encyclopedia - Acute spinal cord injury. [Online]. Available: http://www.urmc.rochester.edu/Encyclopedia/

[70] M. Jesel, J. Deviller, and R. Ottinger, "Lumbo-sacral pinal cord injuries," *Paraplegia*, vol. 18, pp. 351–357, 1980.

[71] W. Reed, *Care of the Combat Amputee - Textbooks of Military Medicine*. Dept. of the Army, 2011.

[72] J. Scott, D. Warburton, D. Williams, S. Whelan, and A. Krassioukov, "Challenges, concerns and common problems: physiological consequences of spinal cord injury and microgravity," *Spinal Cord*, vol. 49, no. 1, pp. 4–16, 2011.

[73] P. Wing, W. Dalsey, E. Alvarez, C. Bombardier, S. Burns, M. Fitzpatrick, D. Green, J. Huff, M. Kincaid, K. Lucke, L. Napolitano, K. Poelstra, A. Vaccaro, J. Wilberger,

and L. Wuermser, "Early acute management in adults with spinal cord injury," *The Journal of Spinal Cord Medicine*, vol. 31, no. 4, pp. 408–479, 2008.

[74] W. McKay, H. Lim, M. Priebe, D. Stokic, and A. Sherwood, "Clinical neurophysiological assessment of residual motor control in post-spinal cord injury paralysis," *Neurorehabilitation and Neural Repair*, vol. 18, no. 3, pp. 144–153, 2004.

[75] C. Winslow and J. Rozovsky, "Effect of spinal cord injury on the respiratory system," *American Journal of Physical Medicine and Rehabilitation*, vol. 82, no. 10, pp. 803–814, 2003.

[76] C. Ho, L. Wuermser, M. Priebe, A. Chiodo, W. Scelza, and S. Kirshblum, "Spinal cord injury medicine. 1. Epidemiology and classification," *Archives of Physical Medicine and Rehabilitation*, vol. 88, no. 3, pp. S49–S54, 2007.

[77] P. New and R. Marshall, "International spinal cord injury data sets for non-traumatic spinal cord injury," *Spinal Cord*, vol. 52, no. 2, pp. 123–132, 2014.

[78] W. Westcott and R. Sheryl, "Spinal cord injury," *Strength and Conditioning Journal*, vol. 32, no. 6, pp. 16–18, 2010.

[79] J. McDonald and C. Sadowsky, "Micro-Doppler effect in radar: phenomenon, model, and simulation study," *The Lancet*, vol. 42, no. 1, pp. 2–21, 2006.

[80] J. Reid and M. Spencer, "Ultrasonic Doppler technique for imaging blood vessels," *Science*, vol. 176, no. 4040, pp. 1235–1236, 1972.

[81] H. White and B. Venkatesh, "Applications of transcranial Doppler in the ICU: a review," *Intensive Care Medicine*, vol. 32, no. 7, pp. 981–94, 2006.

[82] J. Alastruey, K. Parker, J. Peiró, S. Byrd, and S. Sherwin, "Modelling the circle of Willis to assess the effects of anatomical variations and occlusions on cerebral flows," *Journal of Biomechanics*, vol. 40, no. 8, pp. 1794–1805, 2007.

[83] A. Alexandrov, M. Sloan, L. Wong, C. Douville, A. Razumovsky, W. Koroshetz, M. Kaps, and C. Tegeler, "Practice standards for transcranial Doppler ultrasound: part i– test performance," *Journal of Neuroimaging*, vol. 17, no. 1, pp. 11–18, 2007.

[84] S. Duschek and R. Schandry, "Cognitive performance and cerebral blood flow in essential hypotension," *Psychophysiology*, vol. 41, no. 6, pp. 905–913, 2004.

[85] D. Droste, A. Harders, and E. Rastogi, "A transcranial Doppler study of blood flow velocity in the middle cerebral arteries performed at rest and during mental activities," *Stroke*, vol. 20, no. 8, pp. 1005–1011, 1989.

[86] W. Hartje, E. Ringelstein, B. Kistinger, D. Fabianek, and K. Willmes, "Transcranial Doppler ultrasonic assessment of middle cerebral artery blood flow velocity changes

during verbal and visuospatial cognitive tasks," *Neuropsychologia*, vol. 32, no. 12, pp. 1443–1452, 1994.

[87] M. Matteis, U. Bivona, S. Catani, P. Pasqualetti, R. Formisano, F. Vernieri, and E. Troisi, "Functional transcranial Doppler assessment of cerebral blood flow velocities changes during attention tasks," *European Journal of Neurology*, vol. 16, no. 1, pp. 81–87, 2009.

[88] K. Lindegaard, H. Nornes, S. Bakke, W. Sorteberg, and P. Nakstad, "Cerebral vasospasm after subarachnoid haemorrhage investigated by means of transcranial Doppler ultrasound," *Proceedings of the 8th European Congress of Neurosurgery Barcelona, September 6-11, 1987 - Acta Neurochirurgica Supplementum 42*, vol. 42, pp. 81–84, 1988.

[89] D. Evans, W. McDicken, R. Skidmore, and J. Woodcock, *Doppler ultrasound: physics, instrumentation and clinical applications*. John Wiley, Chichester, 1989.

[90] J. Czarske and O. Dolle, "Quadrature demodulation technique used in laser Doppler velocimetry," *Electronics Letters*, vol. 34, no. 6, pp. 547–548, 1998.

[91] R. Cobbold, *Foundations of Biomedical Ultrasound (Biomedical Engineering Series)*. Oxord University Press, 2006.

[92] H. Routh, "Doppler ultrasound," *Engineering in Medicine and Biology Magazine, IEEE*, vol. 15, no. 6, pp. 31–40, 1996.

[93] W. Barber, J. Eberhard, and S. Karr, "A new time domain technique for velocity measurements using Doppler ultrasound," *IEEE Transactions on Biomedical Engineering*, vol. BME-32, no. 3, pp. 213–229, 1985.

[94] M. Anderson, "A heterodyning demodulation technique for spatial quadrature," *Ultrasonics Symposium, 2000 IEEE*, vol. 2, pp. 1487–1490, 2000.

[95] H. Albrecht, N. Damaschke, M. Borys, and C. Tropea, *Laser Doppler and phase Doppler measurement techniques (experimental fluid mechanics)*. Springer, 2002.

[96] D. Zhang, K. Wang, X. Wu, and B. Huang, "Hilbert-Huang transform based Doppler blood flow signals analysis," *Biomedical Engineering and Informatics, 2009. BMEI '09. 2nd International Conference on*, pp. 1–5, 2009.

[97] V. Chen, L. Fayin, and H. Wechsler, "Spinal-cord injury," *IEEE Transactions on Aerospace and Electronic Systems*, vol. 359, no. 9304, pp. 417–425, 2002.

[98] E. Sejdić, D. Kalika, and N. Czarnek, "An analysis of resting-state functional transcranial Doppler recordings from middle cerebral arteries," *PLoS One*, vol. 8, no. 2, 2013.

[99] A. Krassioukov, "Autonomic function following cervical spinal injury," *Respiratory Physiology and Neurobiology*, vol. 169, no. 2, pp. 157–164, 2009.

[100] F. Gonzalez, J. Chang, K. Banovac, D. Messina, A. Martinez-Arizala, and R. Kelley, "Autoregulation of cerebral blood flow in patients with orthostatic hypotension after spinal cord injury," *Paraplegia*, vol. 29, pp. 1–7, 1991.

[101] M. Costa, L. Stegagno, R. Schandry, and P. Ricci Bitti, "Contingent negative variation and cognitive performance in hypotension," *Psychophysiology*, vol. 35, no. 6, pp. 737–744, 1998.

[102] M. Morris, P. Scherr, L. Hebert, D. Bennett, R. Wilson, R. Glynn, and D. Evans, "Association between blood pressure and cognitive function in a biracial community population of older persons," *Neuroepidemiology*, vol. 21, no. 3, pp. 123–130, 2002.

[103] S. Duschek, N. Weisz, and R. Schandry, "Reduced cognitive performance and prolonged reaction time accompany moderate hypotension," *Clinical Autonomic Research*, vol. 13, no. 6, pp. 427–432, 2003.

[104] P. Schneider, M. Rossman, E. Bernstein, S. Torem, E. Ringelstein, and S. Otis, "Effect of internal carotid artery occlusion on intracranial hemodynamics. Transcranial Doppler evaluation and clinical correlation," *Stroke*, vol. 19, no. 5, pp. 589–593, 1988.

[105] A. Papoulis, *Probability, Random Variables, and Stochastic Processes*. New York: WCB/McGraw-Hill, 1991.

[106] J. Hosking, "L-moments: analysis and estimation of distributions using linear combinations of order statistics," *Journal of the royal statistical society. Series B (Methodological)*, vol. 52, no. 1, pp. 105–124, 1990.

[107] A. Zoubir and B. Boashash, "The bootstrap and its application in signal processing," *IEEE Signal Processing Magazine*, vol. 15, no. 1, pp. 56–76, 1998.

[108] J. Allen, J. Coan, and M. Nazarian, "Issues and assumptions on the road from raw signals to metrics of frontal EEG assymetry in emotion," *Biological Psychology*, vol. 67, no. 1-2, pp. 183–218, 2004.

[109] H. Oja, "Descriptive statitics for multivariate distributions," *Statistics and Probability letters*, vol. 1, no. 6, pp. 327–332, 1990.

[110] G. Tiao and G. Box, "Modeling multiple time series with applications," *Journal of the American Statistical Association*, vol. 76, no. 376, pp. 802–816, 1981.

[111] S. Ahmed, M. Shahjahan, and K. Murase, "A Lempel-Ziv Complexity-based neural network pruning algorithm," *International Journal of Neural Systems*, vol. 21, no. 5, pp. 427–441, 2011.

[112] M. Aboy, R. Hornero, D. Abásolo, and D. Álvarez, "Interpretation of the Lempel-Ziv complexity measure in the context of biomedical signal analysis," *IEEE Transactions of Biomedical Engineering*, vol. 53, no. 11, pp. 2282–2288, 2006.

[113] D. Abásolo, R. Hornero, C. Gómez, M. García, and M. López, "Analysis of EEG background activity in Alzeimer's disease patients with Lempel-Ziv complexity and central tendency measure," *Medical Engineering and Physics*, vol. 28, no. 4, pp. 315–322, 2006.

[114] J. Hu, J. Gao, and J. Principe, "Analysis of biomedical signals by the Lempel-Ziv Complexity: the effect of finite data size," *IEEE Transactions on Biomedical Engineering*, vol. 53, no. 12, pp. 2606–2609, 2006.

[115] A. Lempel and J. Ziv, "On the complexity of finite sequences," *IEEE Transactions on Information Theory*, vol. 22, no. 1, pp. 75–81, 1976.

[116] S. Pincus, I. Gladstone, and R. Ehrenkranz, "A regularity statistic fore medical data analysis," *Journal of Clinical Monitoring*, vol. 7, no. 4, pp. 335–345, 1991.

[117] A. Porta, S. Guzzetti, N. Montano, R. Furlan, M. Pagani, and V. Somers, "Entropy, entropy rate, and pattern classification as tools to typify complexity in short heart period variability series," *IEEE Transactions on Information Theory*, vol. 48, no. 11, pp. 1282–1291, 2011.

[118] A. Porta, S. Guzzetti, N. Montano, M. Pagani, V. Somers, A. Malliani, G. Baselli, and S. Cerutti, "Information domain analysis of cardiovascular variability signals: evaluation of regularity, synchronisation and co-ordination," *Medical and Biological Engineering and Computing*, vol. 38, no. 2, pp. 180–188, 2000.

[119] A. Porta, G. Baselli, D. Liberati, N. Montano, C. Cogliati, T. Gnecchi-Ruscone, A. Malliani, and S. Cerutti, "Measuring regularity by means of a corrected conditional entropy in sympathetic outflow," *Biological Cybernetics*, vol. 78, no. 1, pp. 71–78, 1998.

[120] S. Weinstein and P. Ebert, "Data transmission by frequency-division multiplexing using the discrete Fourier transform," *IEEE Transactions onCommunication Technology*, vol. 19, no. 5, pp. 628–634, 1971.

[121] E. Sejdić, I. Djurović, and J. Jiang, "Time-frequency feature representation using energy concentration: an overview of recent advances," *Digital Signal Processing*, vol. 19, no. 1, pp. 153–183, 2009.

[122] J. Lee, E. Sejdić, C. Steele, and T. Chau, "Effects of liquid stimuli on dual-axis swallowing accelerometer signals in a healthy population," *Biomedical Engineering Online*, vol. 9, no. 1, p. 7, 2010.

[123] L. Vergara, J. Gosalbéz, J. Fuente, R. Miralles, and I. Bosch, "Measurement of cement porosity by centroid frequency profiles of ultrasonic grain noise," *Biomedical Engineering Online*, vol. 84, no. 12, p. 2315–2324, 2004.

[124] R. Gao and R. Yan, *Wavelets*. Springer US, 2011.

[125] P. Cox and A. De Carvalho, "Discrete wavelet transform signal analyzer," *IEEE Transactions on Instrumentation and Measurement*, vol. 56, no. 5, pp. 1640–1647, 2007.

[126] M. Hilton, "Wavelet and wavelet packet compression of electrocardiograms," *IEEE Transactions on Biomedical Engineering*, vol. 44, no. 5, pp. 394–402, 1997.

[127] O. Rosso, S. Blanco, J. Yordanova, V. Kolev, A. Figliola, M. Schürmann, and E. Basar, "Wavelet entropy: a new tool for analysis of short duration brain electrical signals," *Journal of Neuroscience Methods*, vol. 105, no. 1, pp. 65–75, 2001.

[128] P. Bridge and S. Sawilowsky, "Increasing physicians' awareness of the impact of statistics on research outcomes: comparative power of the t-test and Wilcoxon rank-sum test in small samples applied research," *Journal of Clinical Epidemiology*, vol. 52, no. 3, pp. 229–235, 1999.

[129] V. DePuy, V. Berger, and Y. Zhou, *Wilcoxon-Mann-Whitney Test. Encyclopedia of Statistics in Behavioral Science*. Wiley, 2005.

[130] G. Hayman, Z. Govindarajulu, F. Leone, P. Kim, and R. Jennrich, *Selected tables in mathematical statistics*. American Mathematical Society, 1970.

[131] L. DeCarlo, "On the meaning and use of kurtosis," *Psychological Methods*, vol. 2, no. 3, pp. 292–307, 1997.

[132] M. Li, H. Huang, M. Boninger, and E. Sejdić, "An analysis of cerebral blood flow from middle cerebral arteries during cognitive tasks via functional transcranial Doppler recordings," *Neuroscience Research*, vol. In press, 2014.

[133] W. Hartje, E. Ringelstein, B. Kistinger, D. Fabianek, and K. Willmes, "Transcranial Doppler ultrasonic assessment of middle cerebral artery blood flow velocity changes during verbal and visuospatial cognitive tasks," *Neuropsychologia*, vol. 32, no. 12, pp. 1443–1452, 1994.

[134] D. Droste, A. Harders, and E. Rastogi, "Two transcranial Doppler studies on blood flow velocity in both middle cerebral arteries during rest and the performance of cognitive tasks," *Neuropsychologia*, vol. 27, no. 10, pp. 1121–1230, 1989.

[135] D. Hirtz, D. Thurman, K. Gwinn-Hardy, M. Mohamed, A. Chaudhuri, and R. Zalutsky, "How common are the "common" neurologic disorders?" *Neurology*, vol. 68, no. 5, pp. 326–337, 2007.

[136] J. Claassen, R. Diaz-Arrastia, K. Martin-Cook, B. Levine, and R. Zhang, "Altered cerebral hemodynamics in early alzheimer disease: a pilot study using transcranial Doppler," *Journal of Alzheimer's disease*, vol. 17, no. 3, pp. 621–629, 2009.

[137] W. Shih, J. Ashford, J. Coupal, Y. Ryo, V. Stipp, S. Magoun, and K. Gross, "Consecutive brain spect surface three-dimensional displays show progression of cerebral cortical abnormalities in alzheimer's disease," *Clinical Nuclear Medicine*, vol. 24, no. 10, p. 773, 1999.

[138] S. Rombouts, R. Goekoop, C. Stam, F. Barkhof, and P. Scheltens, "Delayed rather than decreased BOLD response as a marker for early alzheimer's disease," *NeuroImage*, vol. 26, no. 4, pp. 1078–1085, 2005.

[139] M. Derejko, J. Slawek, D. Wieczorek, B. Brockhuis, M. Dubaniewicz, and P. Lass, "Regional cerebral blood flow in Parkinson's disease as an indicator of cognitive impairment," *Nuclear Medicine Communications*, vol. 27, no. 12, pp. 945–951, 2006.

[140] H. Tachibana, K. Kawabata, Y. Tomino, M. Sugita, and M. Fukuchi, "Brain perfusion imaging in Parkinson's disease and Alzheimer's disease demonstrated by three-dimensional surface display with ^{123}I-Iodoamphetamine," *Dementia and Geriatric Cognitive Disorders*, vol. 4, no. 6, pp. 334–341, 1993.

[141] R. Melrose, M. Ettenhofer, D. Harwood, N. Achamallah, O. Campa, M. Mandelkern, and D. Sultzer, "Cerebral metabolism, cognition, and functional abilities in Alzheimer disease," *Journal of Geriatric Psychiatry and Neurology*, vol. 24, no. 3, pp. 127–134, 2011.

[142] Y. Abe, T. Kachi, T. Kato, Y. Arahata, T. Yamada, Y. Washimi, K. Iwai, K. Ito, N. Yanagisawa, and G. Sobue, "Occipital hypoperfusion in Parkinson's disease without dementia: correlation to impaired cortical visual processing," *Journal of Neurology, Neurosurgery and Psychiatry*, vol. 74, no. 4, pp. 419–422, 2002.

[143] O. Rascol, U. Sabatini, F. Chollet, P. Celsis, J. Montastruc, J. Marc-Vergnes, and A. Rascol, "Supplementary and primary sensory motor area activity in Parkinson's disease: regional cerebral blood flow changes during finger movements and effects of apomorphine," *Archives of Neurology*, vol. 49, no. 2, pp. 144–148, 1992.

[144] M. Firbank, S. Colloby, D. Burn, I. McKeith, and J. O'Brien, "Regional cerebral blood flow in Parkinson's disease with and without dementia," *NeuroImage*, vol. 20, no. 2, pp. 1309–1319, 2003.

[145] S. S., *Gray's Anatomy: the anatomical basis of clinical practice*. Churchill Livingstone, 2008.

[146] M. George, D. Costa, K. Kouris, H. Ring, and P. Ell, "Cerebral blood flow abnormalities in adults with infantile autism," *Journal of Nervous and Mental Disease*, vol. 180, no. 7, pp. 413–417, 1992.

[147] T. Ohnishi, H. Matsuda, T. Hashimoto, T. Kunihiro, M. Nishikawa, T. Uema, and M. Sasaki, "Abnormal regional cerebral blood flow in childhood autism," *Brain*, vol. 123, no. 9, pp. 1838–1844, 2000.

[148] P. Escalante-Mead, N. Minshew, and J. Sweeney, "Abnormal brain lateralization in high-functioning autism," *Journal of Autism and Developmental Disorders*, vol. 33, no. 5, pp. 539–543, 2003.

[149] L. Burroni, A. Orsi, L. Monti, Y. Hayek, R. Rocchi, and A. Vattimo, "Regional cerebral blood flow in childhood autism: a SPET study with SPM evaluation," *Nuclear Medicine Communications*, vol. 29, no. 2, pp. 150–156, 2008.

[150] G. Dawson, "Cerebral lateralization in individuals diagnosed as autistic in early childhood," *Brain and Language*, vol. 15, no. 2, pp. 353–368, 1982.

[151] R. Fisher, W. vn Emde Boas, W. Blume, C. Elger, P. Genton, P. Lee, and J. Engel, "Epileptic seizures and epilepsy: definitions proposed by the International League Against Epilepsy (ILAE) and the I nternational Bureau for Epilepsy (IBE), year = 2005," *Epilepsia*, vol. 46, no. 4, pp. 470–472.

[152] H. Bode, "Intracranial blood flow velocities during seizures and generalized epileptic discharges," *European Journal of Pediatrics*, vol. 151, no. 9, pp. 706–709, 1992.

[153] B. Diehl, R. Diehl, S. Stodieck, and E. Bernd Ringelstein, "Spontaneous oscillations in cerebral blood flow velocities in middle cerebral arteries in control subjects and patients with epilepsy," *Stroke*, vol. 28, no. 12, pp. 2457–2459, 1997.

[154] E. Joo, W. Tae, and S. Hong, "Cerebral blood flow abnormality in patients with idiopathic generalized epilepsy," *Journal of Neurology*, vol. 255, no. 4, pp. 520–525, 2008.

[155] J. Adcock, R. Wise, J. Oxbury, and P. Matthews, "Quantitative fMRI assessment of the differences in lateralization of language-related brain activation in patients with temporal lobe epilepsy," *NeuroImage*, vol. 18, no. 2, pp. 423–438, 2003.

[156] R. Everts, A. Harvey, L. Lillywhite, J. Wrennall, D. Abbott, L. Gonzalez, M. Kean, G. Jackson, and V. Anderson, "Language lateralization correlates with verbal memory performance in children with focal epilepsy," *Epilepsia*, vol. 51, no. 4, pp. 627–638, 2010.

[157] S. Knecht, M. Deppe, B. Drager, L. Bobe, H. Lohmann, E. Ringelstein, and H. Henningsen, "Language lateralization in healthy right-handers," *Brain*, vol. 123, no. 1, pp. 74–81, 2000.

[158] R. Dowler, S. O'Brien, K. Haaland, D. Harrington, F. Feel, and K. Fiedler, "Neuropsychological functioning following a spinal cord injury," *Applied Neuropsychology*, vol. 2, no. 3/4, pp. 124–126, 1995.

[159] J. Soustiel, T. Glenn, V. Shik, J. Boscardin, E. Mahamid, and M. Zaaroor, "Monitoring of cerebral blood flow and metabolism in traumatic brain injury," *Journal of Neurotrauma*, vol. 22, no. 9, pp. 955–965, 2005.

[160] O. Bonne, A. Gilboa, Y. Louzoun, O. Kempf-Sherf, Y. Katz, M. ad Fishman, Z. Ben-Nahum, Y. Krausz, M. Bocher, H. Lester, R. Chisin, and B. Lerer, "Cerebral blood flow in chronic symptomatic mild traumatic brain injury," *Psychiatry Research Neuroimaging*, vol. 124, no. 3, pp. 141–152, 2003.

[161] J. Ghajar, "Traumatic brain injury," *The Lancet*, vol. 356, no. 9233, pp. 923–929, 2000.

[162] A. Marmarou, R. Anderson, J. Ward, S. Choi, H. Young, H. Eisenberg, M. Foulkes, L. Marshall, and J. Jane, "Impact of ICP instability and hypotension on outcome in patients with severe head trauma," *Journal of Neurosurgery*, vol. 75, no. 1s, pp. S59–S66, 1991.

[163] T. Rasmussen and B. Milner, "The role of early left-brain injury in determining lateralization of cerebral speech functions," *Annals of the New York Academy of Sciences*, vol. 299, pp. 355–369, 1977.